International Journal of Heat and Mass Transfer 103 (2016) 753–772

Contents lists available at ScienceDirect

International Journal of Heat and Mass Transfer

journal homepage: www.elsevier.com/locate/ijhmt

An improved interface preserving level set method for simulating three dimensional rising bubble

C.H. Yu [a], Z.T. Ye [a], Tony W.H. Sheu [b,c,d], Y.T. Lin [a], X.Z. Zhao [a,*]

[a] Ocean College, Zhejiang University, 866 Yuhangtang Road, Hangzhou, Zhejiang, People's Republic of China
[b] Department of Engineering Science and Ocean Engineering, National Taiwan University, No. 1, Section 4, Roosevelt Road, Taipei, Taiwan, Republic of China
[c] Institute of Mathematical and Applied Mathematics, National Taiwan University, Taiwan, Republic of China
[d] Center for Advanced Study on Theoretical Sciences (CASTS), National Taiwan University, Taiwan, Republic of China

ARTICLE INFO

Article history:
Received 27 March 2016
Received in revised form 22 July 2016
Accepted 25 July 2016
Available online 11 August 2016

Keywords:
Interface preserving level set method
Bubble rising
Improved smoothed Heaviside function
Mass conservation term
Re-initialization equation
Surface tension force

ABSTRACT

A new interface preserving level set method is developed in three steps to simulate bubble rising problems. In the first step of the solution algorithm, the level set function ϕ is advected by a pure advection equation. An intermediate step is performed to obtain new level set function through an improved smoothed Heaviside function. To keep the new level set function as a distance function and to conserve mass bounded by the interface, in the final solution step a mass correction term is added to the re-initialization equation. This two-phase numerical model is developed underlying the projection method to compute the incompressible Navier–Stokes solutions in collocated grids. In the discretizations of the level set advection equation and the re-initialization equation, the fifth-order weighted essentially non-oscillatory scheme is applied to prevent numerical oscillations occurring around discontinuous interface. The performance of the proposed level set method in conserving mass is compared with conventional level set method applied to solve the single bubble rising problem and the bubble bursting problem at a free surface. Merger of two bubbles is also investigated. Numerical results show that not only the surface tension force can be accurately calculated but also the mass can be conserved excellently using the present level set method.

1. Introduction

Bubble deformation, coalescence and breakup are widely encountered in science and in many industrial processes. Typical examples include propeller cavitation, heat and mass transfer between boiling liquid and bubbles, bubble formation resulting from underwater explosion and entrainment of wave breaking. Bubble motion in liquid fluids is strongly nonlinear, and the deformation of interface can be quite severe when flow is in motion. Therefore, numerical simulation of bubble motion becomes increasingly concerned by researchers of different disciplines. Investigation into bubble rising motion must take into account mass conservation and surface tension force, which play important roles and pose grand computational challenges [1]. In this study, attention will be addressed on the development of incompressible two-phase flow solver, which is applied to predict air/water interface accurately with the surface tension force being considered. Meanwhile, this algorithm can conserve mass as well in the prediction of interface movement.

Interface tracking and interface capturing methods have been widely adopted to model two-phase flows [1]. The interface tracking method [2,3], implemented on a moving surface mesh, has been well known to be very effective in modeling a small interface deformation. However, the re-meshing procedure is computationally expensive when interface undergoes a significant deformation. Another major drawback of the interface tracking methods is that they have difficulty to model bubble coalescence and breakup. Therefore, it is computationally intensive and difficult to apply these methods to study bubble and droplet dynamics [4]. The interface capturing methods, such as the volume of fluid (VOF) methods and the level set (LS) methods, have been developed to simulate two-phase flows in a fixed grid since application of these methods can capture a greater topological change.

In the VOF method, the interface is defined in cells in which the magnitude of the volume fraction F is between zero and unity. The advantage of VOF method is its conservative nature. Hirt and Nichols [5] proposed an original VOF method, which belongs to the algebraic-type of VOF methods. They employed a donor–accep-

* Corresponding author. Fax: +86 571 88208890.
E-mail address: xizengzhao@zju.edu.cn (X.Z. Zhao).

http://dx.doi.org/10.1016/j.ijheatmasstransfer.2016.07.096
0017-9310/

tor formulation with flux limit manipulations to guarantee the boundedness of the numerical solution. Algebraic-type VOF methods always use high resolution schemes to compute volume fraction so that these approaches can normally render a highly diffusive interface and affect the accuracy of the solution. Different from algebraic-type VOF methods, the so-called geometrical-type VOF methods which add an extra step to identify the interface at new position (geometrical reconstruction) are developed. The widely used geometrical-type VOF method are the SLIC (Simple Line Interface Calculation) [6] and the PLIC (Piecewise Linear Interface Calculation) [7–9]. A PLIC scheme is more accurate than a SLIC scheme but it suffers a considerable algorithmic complexity. Another disadvantage of VOF method is that it is more difficult to calculate some geometric properties such as the unit normal vector, curvature and surface tension force along interface from the VOF function, which is defined as the fraction of the volume within each cell of fluids in a discontinuous fashion. An inaccurate calculation of these geometric properties can cause an imbalanced surface tension force to occur and it can furthermore lead to unphysical flow phenomena [10]. To reduce oscillatory and smear-

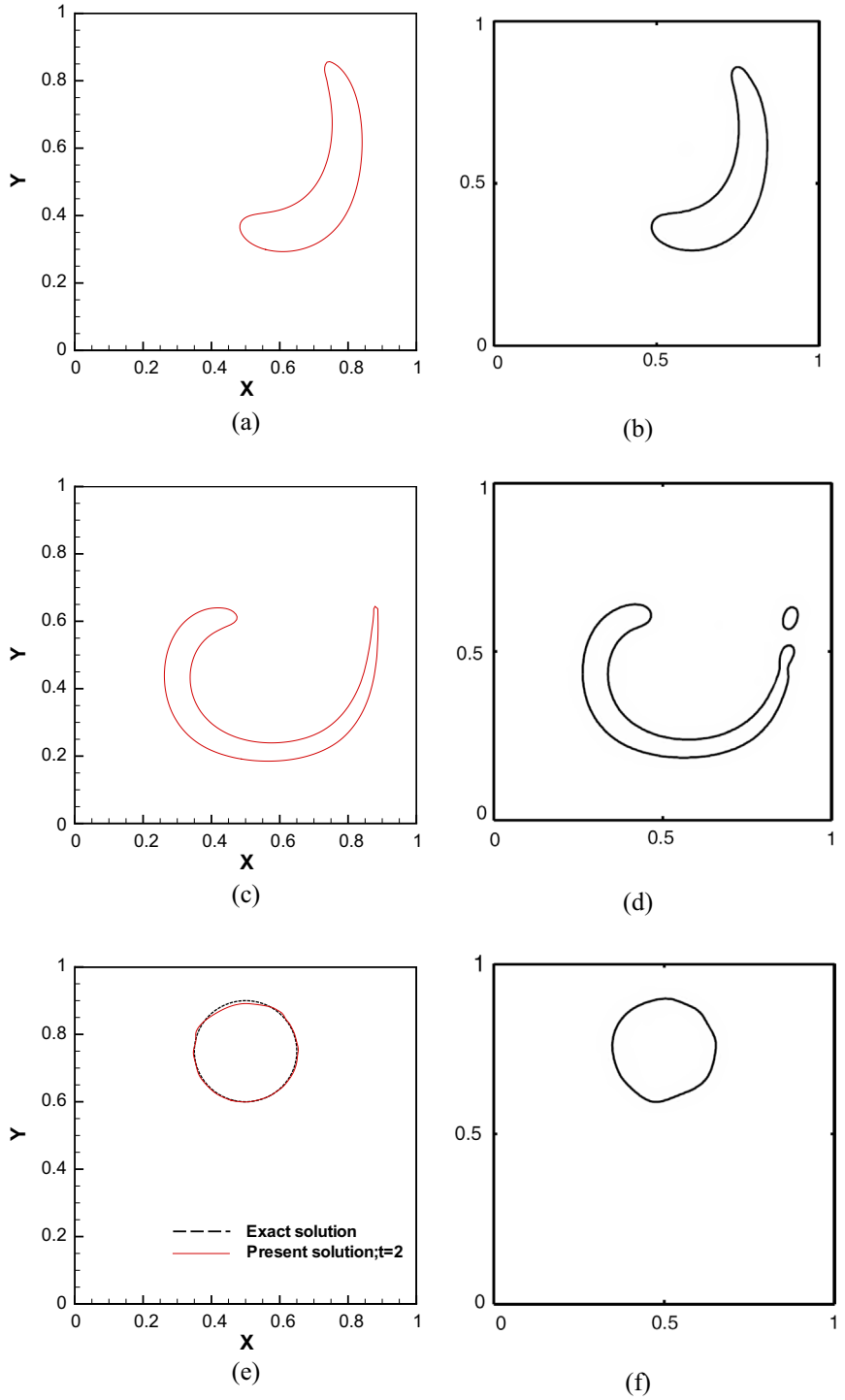

Fig. 1. The predicted interfaces in 128 × 128 grids at. (a) $t = 0.5$; (b) $t = 0.5$ [23]; (c) $t = 1.0$; (d) $t = 1.0$ [23]; (e) $t = 2.0$; (f) $t = 2.0$ [23].

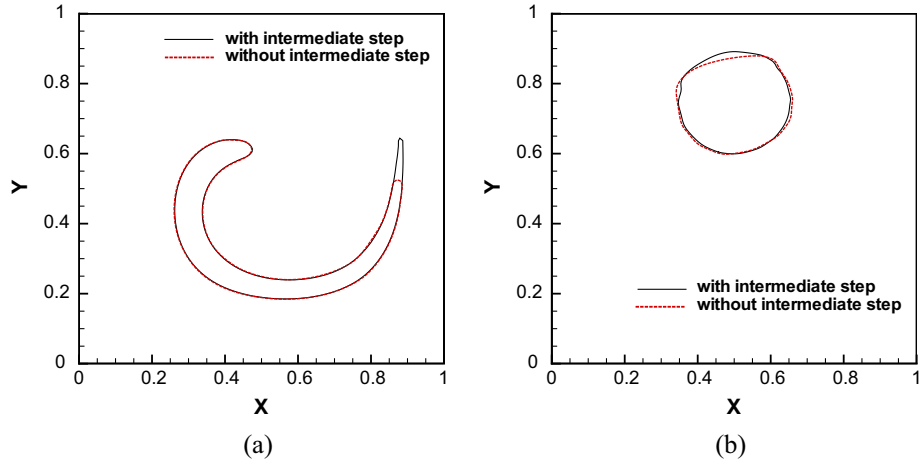

Fig. 2. The predicted solutions of $\phi = 0$ in 128×128 grids with/without using the intermediate step. (a) $t = 1.0$; (b) $t = 2.0$.

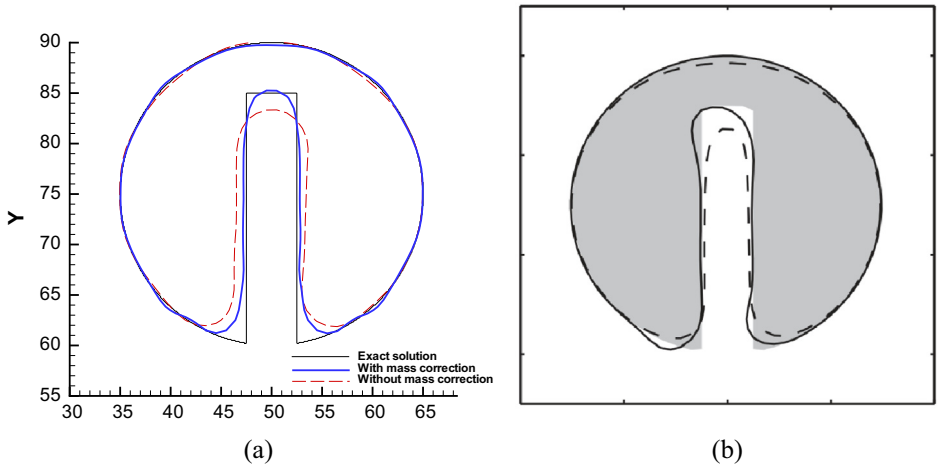

Fig. 3. The contours of $\phi = 0$ predicted in 100×100 grids at a time after one revolution. (a) Present level set method; (b) Mass conservation level set method (dashed line: without mass conservation, solid line: with mass conservation) [22]. Note that re-initialization step is performed at each $128\Delta t$ for the presnet level set method.

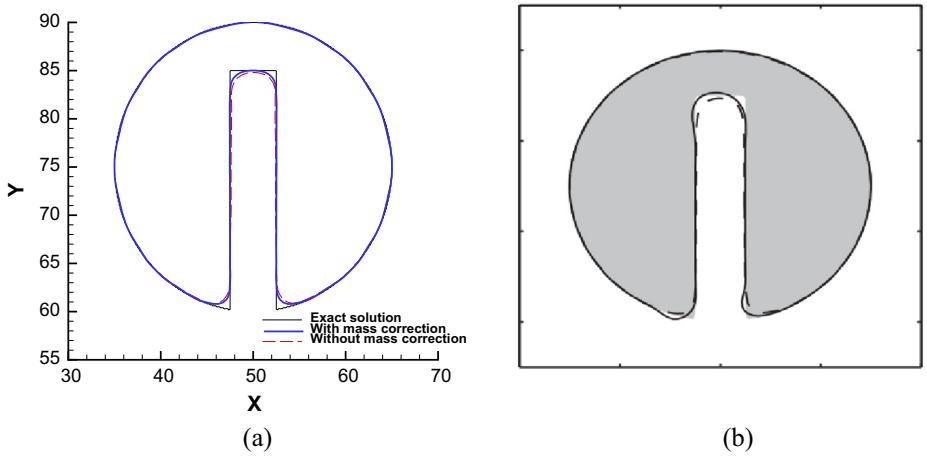

Fig. 4. The contours of $\phi = 0$ predicted in 200×200 grids at a time after one revolution. (a) Present level set method; (b) Mass conservation level set method (dashed line: without mass conservation, solid line: with mass conservation) [22].

ing solutions, the algebraic-type VOF method (i.e. Tangent of Hyperbola for INterface Capturing, THINC) which uses the hyperbolic tangent function to compute the numerical flux for the volume fraction [11–14]. In [15], the THINC method with multi-dimensional reconstruction algorithms that have been developed to suppress spurious current for drop oscillation and bubble rising problems. Advantages of this scheme are that the geometric reconstruction is not required, quadratic surface can

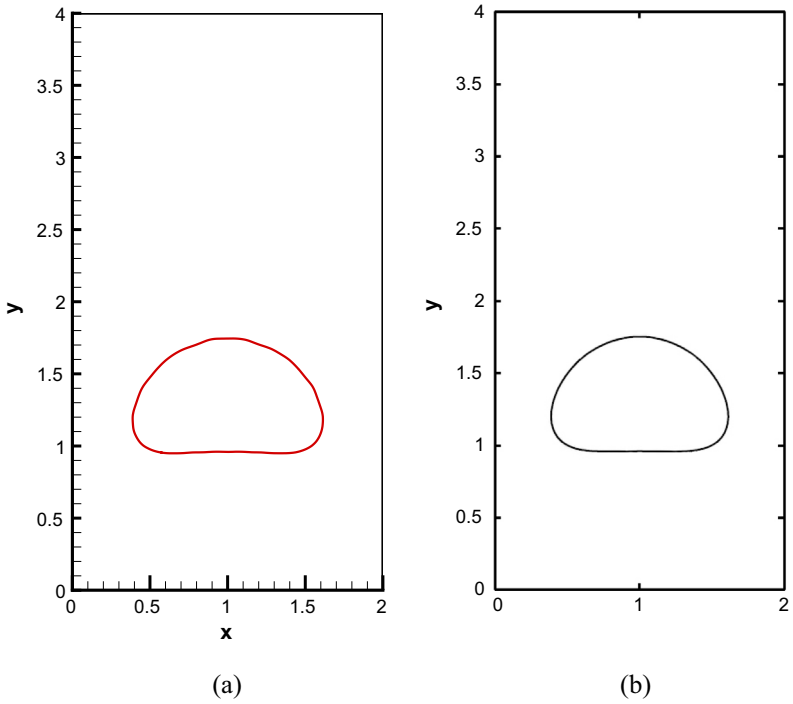

Fig. 5. Comparison of the predicted time-evolving bubble interfaces, obtained in 200 × 400 grids, with those of in [23] for the case taking the surface tension into account. (a) $t = 0.5$; (b) $t = 0.5$ [23].

be constructed easily, and the derivatives and normal vectors can be calculated directly through the continuous multi-dimensional hyperbolic tangent function.

For the level set methods [16–21], the interface can be defined by zero contour of a continuously signed distance function so that the curvature of interface can be easily calculated due to the smooth nature of the level set function across interface. As time goes by, the level set function becomes increasingly irregular. To retain the level set function as a signed distance function, the re-initialization procedure is required to perform. Thus, a small amount of mass may be lost or gained in this process. The difficulty of maintaining a good mass conservation is now known as the major drawback of the level set approach. Many researchers have proposed different ways to conserve mass within the framework of level set methods. A mass-conserving level-set (MCLS) method is proposed to model bubble dynamics [22]. In this model, the level set method is adopted to calculate the surface tension force, and VOF function is used to conserve mass when interface is advected in the flow. The modified level set method with the built-in conservative property, known as the conservative level set method, is developed to improve mass conservation [23,24]. In their modified level set methods, in the intermediate solution step both artificial compression and viscosity terms are added to sharpen interface and to avoid small interface thickness, respectively. More works of improving conservative level set methods can be found in Strubelj and Tiselj [25] and Ng et al. [26]. In [27,28], a global mass correction scheme for the level set method is developed to study bubble evolution. In their studies, the third distance function is introduced to ensure mass conservation. This method can be further applied to predict the trajectory of a solid object entering and exiting the water body [29].

Based on the above analysis of the VOF and LS methods, one can take advantages of both methods to develop a method combining the VOF method with the LS method. In [1,4,30–35], a coupled level set and volume-of-fluid (CLSVOF) method exploiting full advantages of the VOF and LS methods is developed. In this coupled method, the interface is approximated in a piecewise linear manner, which is reconstructed from the VOF approach, and the normal vector, curvature and surface tension force of interface are calculated from the smooth level set function. This coupled method is popular in the simulation of two-phase flows because of its potential of yielding a better mass conservation and a more accurate calculation of geometric properties. As is mentioned above, LS, VOF or CLSVOF methods are all designed to capture the moving surface. Note that CLSVOF method can be seen as an improvement on each individual scheme (VOF and LS), aiming to combine their merits. CLSVOF method, unfortunately, inevitably encounters complex interface reconstruction and may suffer a computational burden and involve difficulties in programming. Development of a more efficient and accurate algorithm for CLSVOF method is still needed. Another approach proposed to ensure mass conservation is called a coupled volume of fluid and level set (VOSET) method for the calculation of incompressible two-phase flows [36]. In this method, VOF approach is adopted to capture interfaces to conserve mass. In addition, an iterative geometric approach is proposed to calculate the level set function, which can be applied to compute more accurately the geometric properties and to resolve the physically sharp interface without incurring contact discontinuous oscillations. More computational examples of the interfacial flows can be found in the relatively new and efficient VOSET method [37,38].

In the present work, the main objective is to adopt the interface preserving level set method [39] to improve the degree of mass conservation and to calculate surface tension force more accurately in arbitrarily shaped interfaces which may be merged or split. We first calculate the level set function from the new smoothed Heaviside function after solving the advection equation for the level set function. Then, the re-initialization equation is modified by adding a correction term to preserve mass conservation in a sharp interface region. The outline of this paper is described as follows: In Section 2.1, new smoothed Heaviside function will be designed to smoothen fluid viscosity and density profiles. Section 2.2 describes an improved interface preserving level set method. Numerical pro-

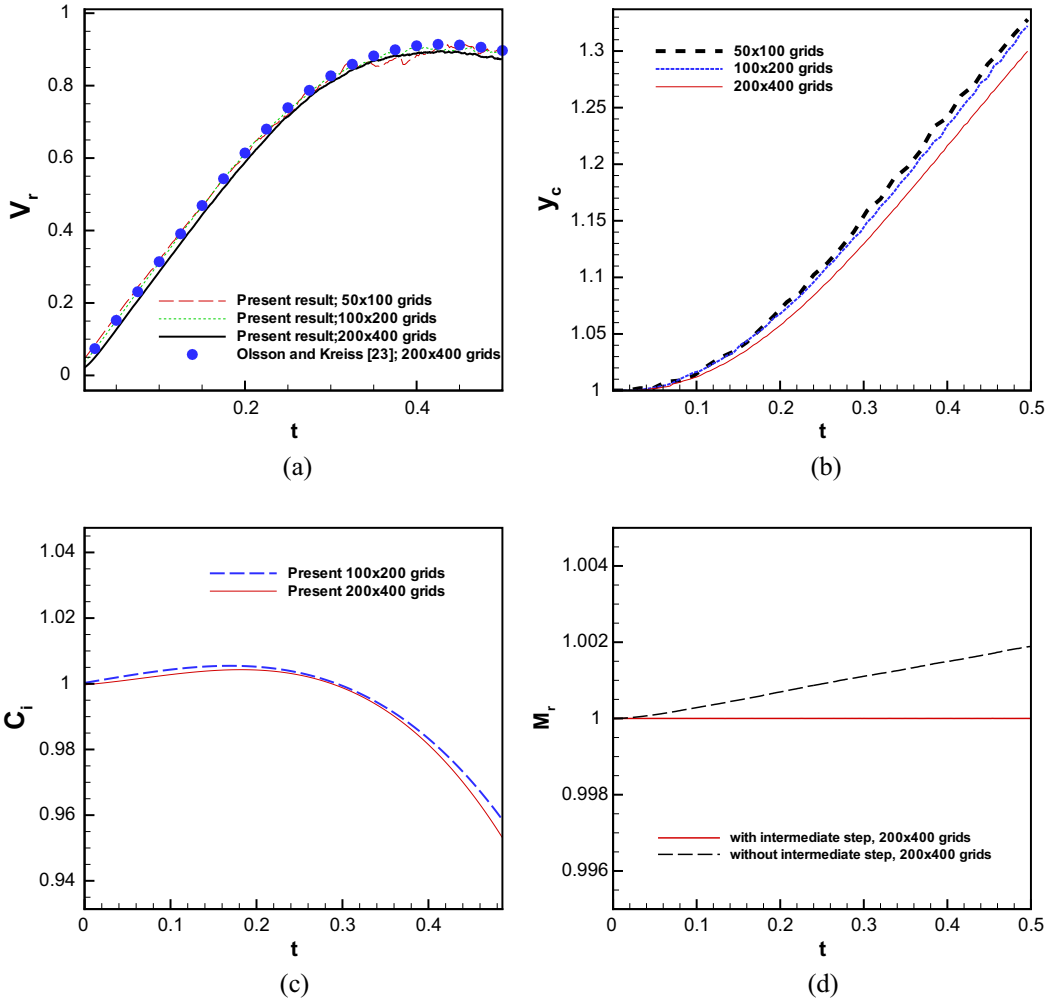

Fig. 6. The plot of the predicted benchmark quantities against the dimensionless time for the 2D bubble rising problem described in Section 4.2.1. (a) rise velocity; (b) center of mass; (c) circularity; (d) mass ratio.

Table 1
Comparison of the solution algorithms for the calculations performed in different grids with/without using the intermediate step. This problem is described in Section 4.2.1.

	Grids	Mass conservation	CPU times (s)
Without intermediate step	50×100	No	58.0
	100×200	No	471.2
	200×400	No	3615.6
With intermediate step	50×100	Yes	61.6
	100×200	Yes	489.9
	200×400	Yes	3645.3

cedures and schemes are presented in Section 3. Section 4 investigates the bubble rising motion in a container partially filled with water, single bubble rising in a container, and two-bubble merging problem. Finally, we will draw some conclusions in Section 5.

2. Numerical modeling

2.1. Smooth Heaviside function and delta function

The jumps of ρ and μ across an interface need to be smoothed in order to avoid contact discontinuities occurring in regions near the interface. To prevent unphysical oscillations, both density and viscosity are smoothly distributed across the interface by employing the smoothed Heaviside function $\mathcal{H}(\phi)$, thereby leading to

$$\rho(\phi) = \rho_G + (\rho_L - \rho_G)\mathcal{H}(\phi), \tag{1}$$

$$\mu(\phi) = \mu_G + (\mu_L - \mu_G)\mathcal{H}(\phi), \tag{2}$$

with $\mathcal{H}$ being chosen as follows

$$\mathcal{H}(\phi) = \begin{cases} 0; & \text{if } \phi < -\varepsilon \\ \dfrac{1}{\left(1+e^{-\frac{3\phi}{\varepsilon}}\right)}; & \text{if } |\phi| \leqslant \varepsilon \\ 1; & \text{if } \phi > \varepsilon \end{cases} \tag{3}$$

The subscripts G and L shown in Eqs. (1) and (2) represent the air and water phases, respectively. The level set function ϕ is defined as the signed distance function from the interface. The smoothed delta function $\delta(\phi)$ obtained from $\frac{d\mathcal{H}(\phi)}{d\phi}$ is as follows

$$\delta(\phi) = \begin{cases} \dfrac{3e^{-\frac{3\phi}{\varepsilon}}}{\left(1+e^{-\frac{3\phi}{\varepsilon}}\right)^2 \varepsilon}; & \text{if } |\phi| \leqslant \varepsilon \\ 0; & \text{otherwise.} \end{cases} \tag{4}$$

It is noted that the width of interface region ε is chosen as $1.5\Delta x$, where Δx is the gird spacing.

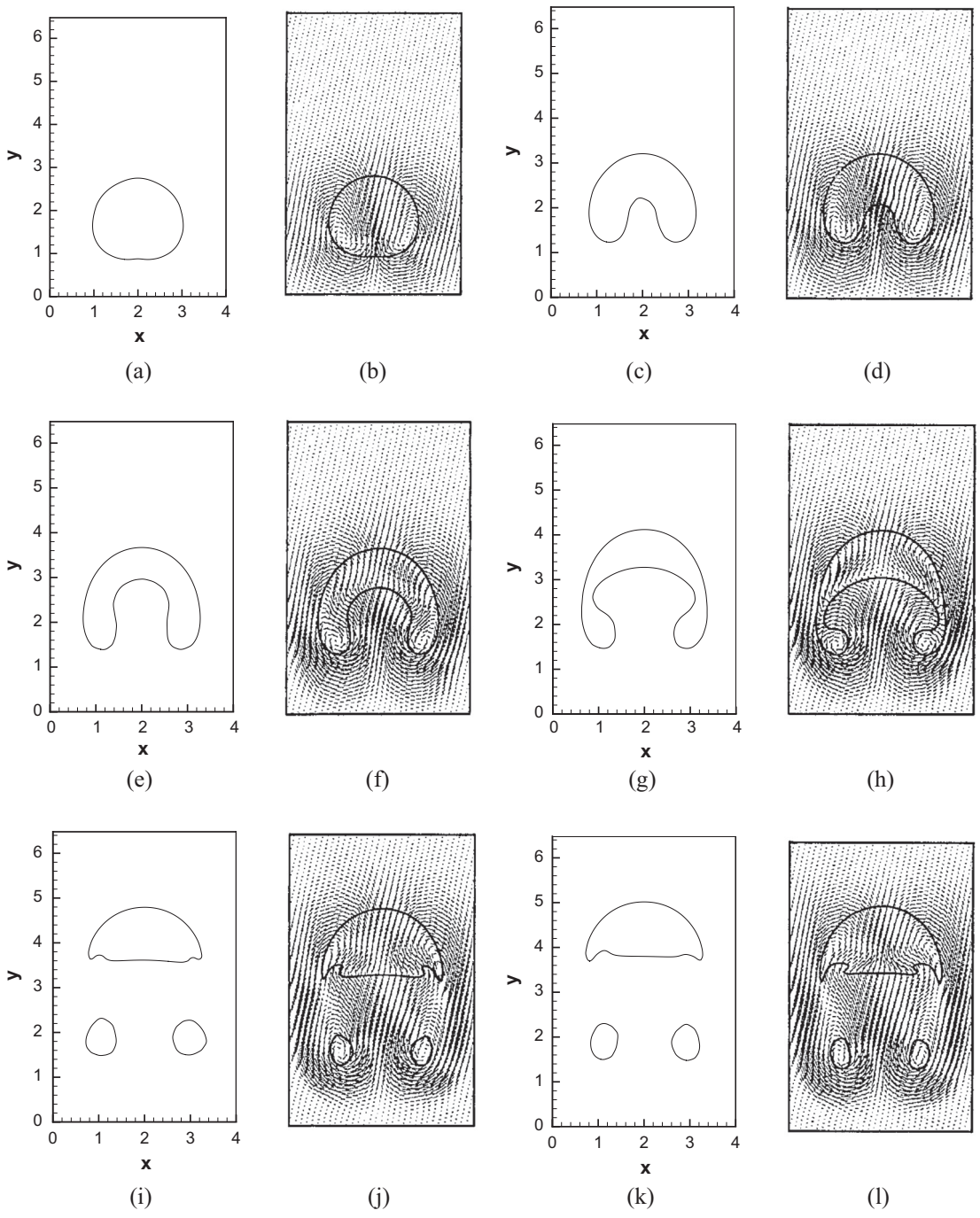

Fig. 7. The predicted results for a single bubble rising problem for the case with $Re = 100, We = 200$ and $\frac{\rho_G}{\rho_L} = 0.01$ at different dimensionless times. (a) $t = 1$; (b) $t = 1$ [48]; (c) $t = 2$; (d) $t = 2$ [48]; (e) $t = 3$; (f) $t = 3$ [48]; (g) $t = 4$; (h) $t = 4$ [48]; (i) $t = 5.5$; (j) $t = 5.5$ [48]; (k) $t = 6$; (l) $t = 6$ [48].

2.2. Improved interface preserving level set method

The proposed three-step solution algorithm aiming at accurately predicting interface is described below.

2.2.1. Advection step

In the adopted level set method, the level set function ϕ is initially prescribed to have the signed distance values given below

$$\phi = \begin{cases} -d & for \quad x \in \Omega_{air} \\ 0 & for \quad x \in \Gamma_{interface} \\ d & for \quad x \in \Omega_{water}. \end{cases} \tag{5}$$

Here, d denotes the absolute normal distance to the interface. An interface separating air and water can be regarded as the evolution of the zero level set function (i.e. $\phi = 0$) governed by

$$\phi_t + \mathbf{u} \cdot \nabla \phi = 0. \tag{6}$$

It is implied that interface will be advected with the flow velocity vector $\mathbf{u}$. Given the mass conservation property $\int \mathcal{H}(\phi) d\Omega$, where Ω is any fixed domain, should be mass conserved all the time (i.e. $\int \mathcal{H}(\phi, t = 0) d\Omega = \int \mathcal{H}(\phi, t) d\Omega$). However, in actual computation of Eq. (6), the applied scheme will introduce numerical error that will more or less deteriorate the predicted solution of level set function as time proceeds (i.e.

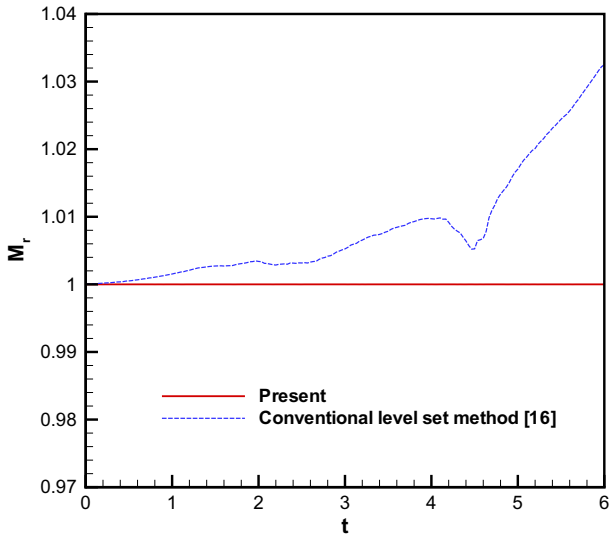

Fig. 8. The ratios $\mathbf{M}_r$ defined in Eq. (38) are plotted with respect to the dimensionless time t for a single bubble rising problem predicted at $Re = 100, We = 200$ and $\frac{\rho_G}{\rho_L} = 0.01$.

$\int \mathcal{H}(\phi, t=0)d\Omega - \int \mathcal{H}(\phi,t)d\Omega = \mathcal{H}_{error} \neq 0$). To retain the mass conservation property, the procedure described in the following intermediate step is essential.

2.2.2. Intermediate step

For retaining the mass conservation property, we introduce

$$\mathcal{H}(\phi_{new},t) = \begin{cases} \mathcal{H}(\phi,t) + \frac{|\mathcal{H}_{error}|\mathbf{sgn}(\mathcal{H}_{error})}{\sum \mathbf{N}}; & \text{if } 0 < \mathcal{H}(\phi,t) < 1, \\ \mathcal{H}(\phi,t); & \text{if } \mathcal{H}(\phi,t) = 0 \text{ or } \mathcal{H}(\phi,t) = 1, \end{cases} \tag{7}$$

where $\mathbf{N}$ denotes the nodal point in the smooth layer (or in the thickness of interface). If $\mathcal{H}(\phi_{new},t) > 1$, set $\mathcal{H}(\phi_{new},t) = 1$; if $\mathcal{H}(\phi_{new},t) < 0$, set $\mathcal{H}(\phi_{new},t) = 0$. The new values of ϕ_{new} can be calculated from the following formulation

$$\phi_{new} = \begin{cases} -\frac{1}{3}\ln(-\frac{\mathcal{H}(\phi_{new},t)-1}{\mathcal{H}(\phi_{new},t)})\varepsilon; & \text{if } 0 < \mathcal{H}(\phi,t) < 1, \\ \phi; & \text{if } \mathcal{H}(\phi,t) = 0 \text{ or } \mathcal{H}(\phi,t) = 1. \end{cases} \tag{8}$$

Note that the new level set function ϕ_{new} can be derived from Eq. (3). This procedure, as a result, guarantees mass conservation inside the thickness of interface.

2.2.3. Re-initialization step

To ensure that ϕ_{new} can remain as a distance function and to conserve mass bounded by the interface, the computed solution ϕ_{new} from Eq. (8) is employed as the initial solution in solving the following re-initialization equation:

$$\phi_\tau = \mathbf{sgn}(\phi_{new})(1 - |\nabla\phi|) + \lambda\delta(\phi)|\nabla\phi|. \tag{9}$$

In the above, τ is a pseudo-time and $\mathbf{sgn}(\phi_{new}) = 2(\mathcal{H}(\phi_{new}) - \frac{1}{2})$, and $\lambda\delta(\phi)|\nabla\phi|$ is the mass correction term. Note that λ can be determined from the interface preserving condition given by [39]

$$\frac{\partial}{\partial t}\int \mathcal{H}(\phi)d\Omega = \int \mathcal{H}'(\phi)\phi_\tau d\Omega = \int \mathcal{H}'(\phi)(\mathbf{sgn}(\phi_{new})(1 - |\nabla\phi|) + \lambda\delta(\phi)|\nabla\phi|)d\Omega = 0. \tag{10}$$

The parameter λ can be thus prescribed as

$$\lambda = -\frac{\int_\Omega \delta(\phi)(\mathbf{sgn}(\phi_{new})(1 - |\nabla\phi|))d\Omega}{\int_\Omega \delta^2(\phi)|\nabla\phi|d\Omega}. \tag{11}$$

Numerical simulation of Eq. (9) has shown that ϕ can be kept as a distance function near interface.

2.3. Coupling of Navier–Stokes equations with level set function

The incompressible two-phase flow equations for the air and water phases are governed by

$$\nabla \cdot \mathbf{u} = 0, \tag{12}$$

$$\rho(\phi)\left(\frac{\partial \mathbf{u}}{\partial t} + \nabla\cdot\mathbf{uu}\right) = -\nabla p + \nabla\cdot\left[\mu(\phi)(\nabla\mathbf{u} + \nabla\mathbf{u}^{\mathbf{T}})\right] + \rho(\phi)\mathbf{g} + \mathbf{f}_{sf}, \tag{13}$$

where $\mathbf{u} = (u, v)$ is the velocity vector, p the pressure and $\mathbf{g} = (0, 0, -g)$ the gravitational acceleration. $\rho(\phi)$ and $\mu(\phi)$ shown in Eq. (13) are the density and viscosity, respectively. In Eq. (13), $\mathbf{f}_{sf}$ is the surface tension force per an interfacial area at a point on the interface. As pointed out in [33,40], in the level set formulation, surface tension force can be written in terms of ϕ as follows by adopting the density-scaled continuum surface force (CSF) model:

$$\mathbf{f}_{sf} = \sigma\kappa(\phi)\delta^{scaling}(\phi)\nabla\phi, \tag{14}$$

where $\delta^{scaling}(\phi) = 2\mathcal{H}(\phi)\delta(\phi)$. In Eq. (14), σ is the fluid surface tension coefficient and is assumed to be a constant, κ is the local mean curvature, and $\mathbf{n}$ is the unit vector normal to the water interface. The gradient of ϕ shown in Eq. (14) can be computed by a central difference scheme. The curvature of the interface, or $\kappa(\phi)$, can be derived as

$$\begin{aligned}\kappa(\phi) &= -\nabla\cdot\left(\frac{\nabla\phi}{|\nabla\phi|}\right) \\ &= -\Big(\phi_x^2\phi_{yy} - 2\phi_x\phi_y\phi_{xy} + \phi_y^2\phi_{xx} + \phi_x^2\phi_{zz} - 2\phi_x\phi_z\phi_{xz} + \phi_z^2\phi_{xx} \\ &\quad + \phi_y^2\phi_{zz} - 2\phi_y\phi_z\phi_{yz} + \phi_z^2\phi_{yy}\Big)\Big/\left(\phi_x^2 + \phi_y^2 + \phi_z^2\right)^{\frac{3}{2}}\end{aligned} \tag{15}$$

3. Numerical schemes and solution algorithm

The key to success in accurately predicting a time varying interface lies in the approximation of the convection terms in the momentum and the level set equations described respectively in Section 3.1 and 3.2. This is followed by the presentation of the entire solution algorithm in Section 3.3.

3.1. Momentum equation solver

The convection terms in the momentum equation are discretized using the third-order QUICK (quadratic upwind interpolation for convective kinematics) scheme [41]. For example, the convection term $\frac{\partial(v\mathbf{u})}{\partial y}$ in the y-direction momentum equation can be approximated as

$$\frac{\partial(v\mathbf{u})}{\partial y} = \frac{v_{i+\frac{1}{2}j}\mathbf{u}_{i+\frac{1}{2}j} - v_{i-\frac{1}{2}j}\mathbf{u}_{i-\frac{1}{2}j}}{\Delta y}, \tag{16}$$

where the value of $\mathbf{u}_{i+\frac{1}{2}j}$ is evaluated as:

$$\mathbf{u}_{i+1/2,i} = \begin{cases} \frac{1}{8}(-u_{i-1,j} + 6u_{ij} + 3u_{i+1,j}), & \text{if } v_{i+1/2,j} \geqslant 0, \\ \frac{1}{8}(-u_{i+2,j} + 6u_{i+1,j} + 3u_{ij}), & \text{if } v_{i+1/2,j} < 0. \end{cases} \tag{17}$$

The diffusion term is approximated by the second-order center difference scheme.

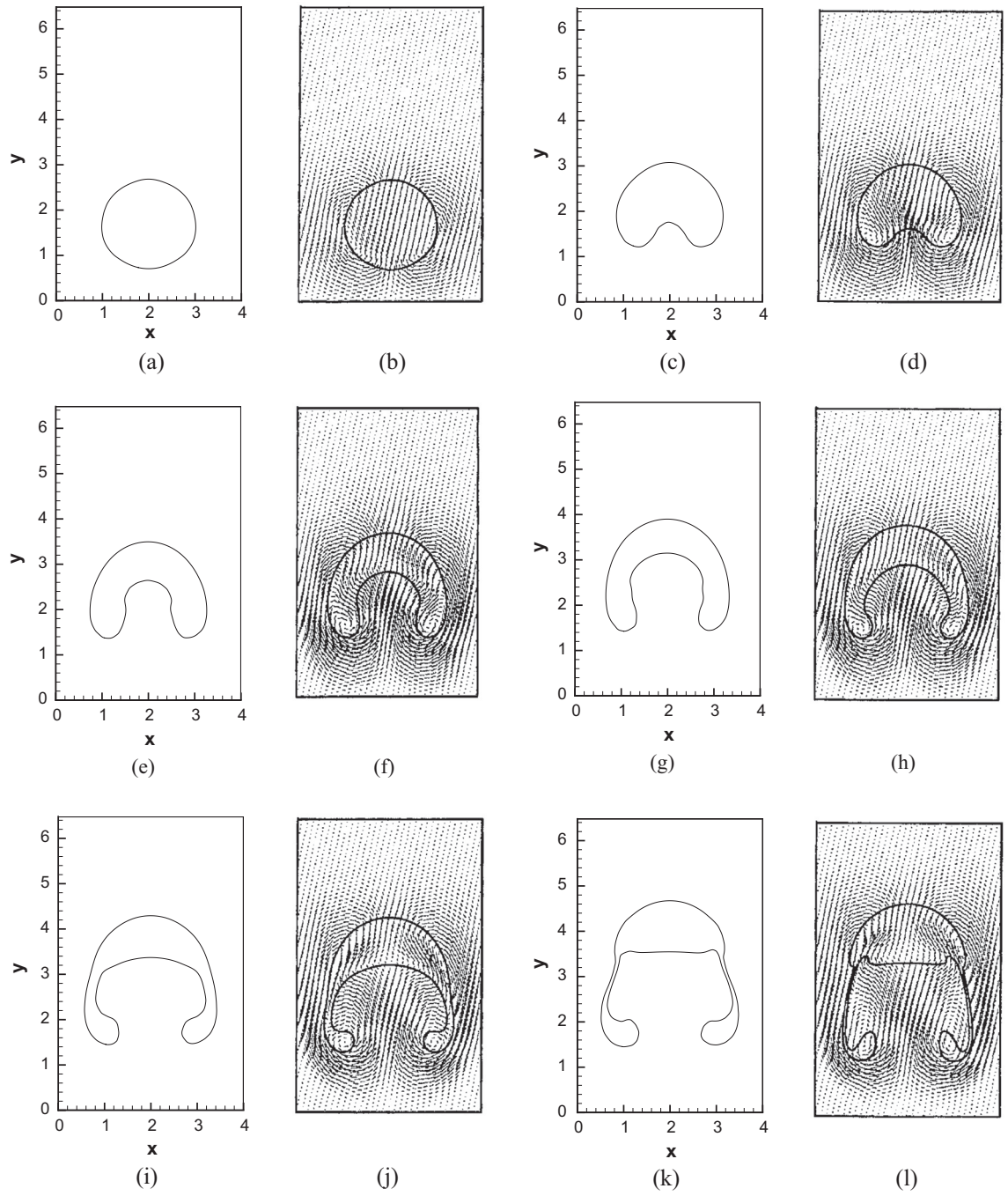

Fig. 9. The predicted results for a single bubble rising problem investigated at $Re = 100, We = 200$ and $\frac{\rho_G}{\rho_L} = 0.2$ at different dimensionless times. (a) $t = 1$; (b) $t = 1$ [48]; (c) $t = 2$; (d) $t = 2$ [48]; (e) $t = 3$; (f) $t = 3$ [48]; (g) $t = 4$; (h) $t = 4$ [48]; (i) $t = 5.5$; (j) $t = 5.5$ [48]; (k) $t = 6$; (l) $t = 6$ [48].

3.2. Level set equation solver

For capturing interface, the fifth-order Hamilton–Jocobi weighted essentially non-oscillatory (HJ-WENO) scheme [42] is used for the approximation of the level set and re-initialization equations. For example, the derivative term $\frac{\partial \phi}{\partial x}$ in Eq. (6) is approximated as

$$(\phi_x)_i = \begin{cases} (\phi_x^-)_i, & \text{if } u_i \geqslant 0, \\ (\phi_x^+)_i, & \text{if } u_i < 0. \end{cases} \tag{18}$$

In Eq. (18), $(\phi_x^-)_i$ and $(\phi_x^+)_i$ are calculated using the nodal values of $\phi_{i-3} \sim \phi_{i+3}$

$$\phi_{x,i}^- = \frac{1}{12}\left(-\frac{\triangle^+\phi_{i-2}}{\triangle x} + 7\frac{\triangle^+\phi_{i-1}}{\triangle x} + 7\frac{\triangle^+\phi_i}{\triangle x} - \frac{\triangle^+\phi_{i+1}}{\triangle x}\right) - \phi^{WENO}\left(\frac{\Delta^-\Delta^+\phi_{i-2}}{\Delta x}, \frac{\Delta^-\Delta^+\phi_{i-1}}{\Delta x}, \frac{\Delta^-\Delta^+\phi_i}{\Delta x}, \frac{\Delta^-\Delta^+\phi_{i+1}}{\Delta x}\right), \tag{19}$$

and

$$\phi_{x,i}^+ = \frac{1}{12}\left(-\frac{\triangle^+\phi_{i-2}}{\triangle x} + 7\frac{\triangle^+\phi_{i-1}}{\triangle x} + 7\frac{\triangle^+\phi_i}{\triangle x} - \frac{\triangle^+\phi_{i+1}}{\triangle x}\right) - \phi^{WENO}\left(\frac{\Delta^-\Delta^+\phi_{i+2}}{\Delta x}, \frac{\Delta^-\Delta^+\phi_{i+1}}{\Delta x}, \frac{\Delta^-\Delta^+\phi_i}{\Delta x}, \frac{\Delta^-\Delta^+\phi_{i-1}}{\Delta x}\right), \tag{20}$$

where $\triangle^+\phi_k = \phi_{k+1} - \phi_k, \triangle^-\phi_k = \phi_k - \phi_{k-1}$ $(k = i-3 \sim i+2)$. Note that $\phi^{WENO}(\mathbf{a}, \mathbf{b}, \mathbf{c}, \mathbf{d})$ can be expressed below in terms of $\mathbf{a}, \mathbf{b}, \mathbf{c}, \mathbf{d}$

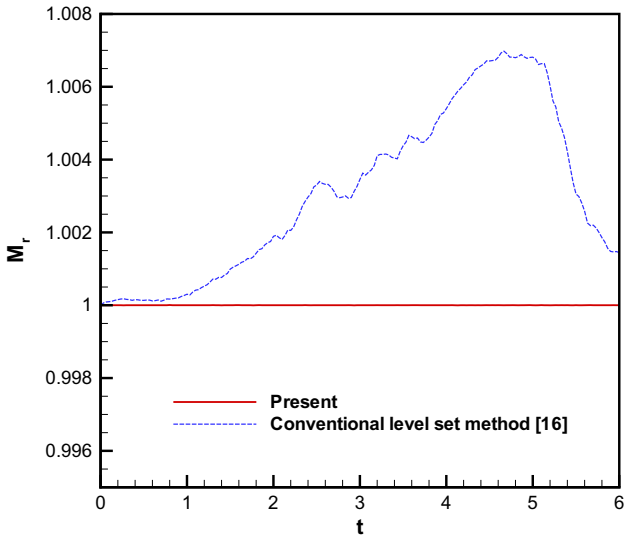

Fig. 10. The ratios $\mathbf{M}_r$ defined in Eq. (38) are plotted with respect to the dimensionless time t for a single bubble rising problem investigated at $Re = 100, We = 200$ and density ratio $\frac{\rho_G}{\rho_L} = 0.2$.

Table 2
Comparison of the solution algorithms for the calculations performed in $60 \times 60 \times 80$ grids with/without using the intermediate step. This problem is described in Section 4.2.3.

	Grids	Mass conservation	CPU times (*s*)
Without intermediate step	$60 \times 60 \times 80$	No	55,976
With intermediate step	$60 \times 60 \times 80$	Yes	56,117

$$\phi^{WENO}(\mathbf{a},\mathbf{b},\mathbf{c},\mathbf{d}) = \frac{1}{3}\omega_0(\mathbf{a}-2\mathbf{b}+\mathbf{c}) + \frac{1}{6}\left(\omega_2 - \frac{1}{2}\right)(\mathbf{b}-2\mathbf{c}+\mathbf{d}). \tag{21}$$

The optimal weights ω_0 and ω_2 in Eq. (21) are defined in [41]

$$\omega_0 = \frac{\alpha_0}{\alpha_0+\alpha_1+\alpha_2}, \quad \omega_2 = \frac{\alpha_2}{\alpha_0+\alpha_1+\alpha_2}, \tag{22}$$

with

$$\alpha_0 = \frac{1}{(\varepsilon+IS_0)^2}, \quad \alpha_1 = \frac{6}{(\varepsilon+IS_1)^2}, \quad \alpha_2 = \frac{3}{(\varepsilon+IS_2)^2}. \tag{23}$$

Note that $\varepsilon = 10^{-6}$ is chosen to prevent division by zero. The smoothness indicators IS_0, IS_1, IS_2 designed below to detect the presence of large discontinuities can automatically switch the stencil to decrease the degree of oscillation in the solution

$$IS_0 = 13(\mathbf{a}-\mathbf{b})^2 + 3(\mathbf{a}-3\mathbf{b})^2,$$
$$IS_1 = 13(\mathbf{b}-\mathbf{c})^2 + 3(\mathbf{b}+\mathbf{c})^2,$$
$$IS_2 = 13(\mathbf{c}-\mathbf{d})^2 + 3(3\mathbf{c}-\mathbf{d})^2.$$

For the approximation of the time derivative term, the explicit total variation diminishing Runge–Kutta (TVD-RK) scheme consisting of the following three solution steps is employed [43]

$$\phi^{(1)} = \phi^{(n)} + \Delta t L(\phi^{(0)}), \tag{24}$$

$$\phi^{(2)} = \frac{3}{4}\phi^{(n)} + \frac{1}{4}\phi^{(1)} + \frac{1}{4}\Delta t L(\phi^{(1)}), \tag{25}$$

$$\phi^{(n+1)} = \frac{1}{3}\phi^{(n)} + \frac{2}{3}\phi^{(2)} + \frac{2}{3}\Delta t L(\phi^{(2)}). \tag{26}$$

3.3. Solution algorithm

An improved interface preserving level set method is developed for getting a better interface representation. The projection method [44] which is an effective method in solving the time-dependent incompressible flow solutions has been performed. The advantage of the projection method employed in this study is that the computation of velocity and pressure fields can be decoupled. The present computational procedures are summarized as follows:

(Step 1) Set $\phi_0 = 1$ in the water (outside the bubble) while $\phi_0 = -1$ in the air (inside the bubble). Initialize the level set function ϕ by solving the initialization equation

$$\phi_\tau + \mathrm{sgn}(\phi_0)(|\nabla\phi| - 1) = 0. \tag{27}$$

Given the solution obtained at a time $T = L_D$, which is the largest length of the computational domain, we set the computed value of ϕ_0 as ϕ.

(Step 2) Define the fluid density $\rho(\phi)$ and viscosity $\mu(\phi)$ according to the level set function ϕ shown in Eqs. (1) and (2).

(Step 3) Calculate the intermediate velocity $\mathbf{u}^*$, which does not necessarily satisfy the divergence-free constraint condition, from the following momentum vector equation without taking the pressure gradient term into account:

$$\frac{\mathbf{u}^* - \mathbf{u}^n}{\Delta t} = -\nabla\cdot\mathbf{u}^n\mathbf{u}^n + \frac{\nabla\cdot(2\mu(\phi)\underline{\underline{\mathbf{D}}}^n)}{\rho(\phi)} + \mathbf{g} - \frac{\sigma\kappa\delta^{scaling}(\phi)\nabla\phi}{\rho(\phi)}, \tag{28}$$

where $\underline{\underline{\mathbf{D}}} = \frac{1}{2}(\nabla\mathbf{u} + \nabla\mathbf{u}^T)$.

(Step 4) Correct the intermediate velocity to obtain the solution at the time step $\mathbf{n}^{n+1}$ by taking into account the pressure gradient term shown below

$$\frac{\mathbf{u}^{n+1} - \mathbf{u}^*}{\Delta t} = -\frac{\nabla p}{\rho(\phi)}. \tag{29}$$

The above equation holds under the constraint equation $\nabla\cdot\mathbf{u}^{n+1} = 0$.

(Step 5) Solve Eq. (6) by the HJ-WENO scheme with the TVD-RK time marching scheme described in Section 3.2 to obtain ϕ^{n+1}.

(Step 6) Calculate the new level set value ϕ^{n+1}_{new} by Eq. (8).

(Step 7) Re-initialize the level set function ϕ^{n+1}_{new} by solving Eq. (9) described in Section 2.2.3.

(Step 8) Repeat the calculations form Step 2 to Step 7 for one time loop.

4. Numerical results

Two benchmark problems including the vortex in a box problem in Section 4.1.1 and the Zalesak's problem in Section 4.1.2 are solved to verify the proposed improved level set method. Furthermore, our numerical method is applied to solve several 2D and 3D two-phase flow problems. In Section 4.2.1, the effect of density and the behavior of bubble splitting are addressed for a single bubble rising problem. In Section 4.2.2, solutions computed from the improved interface preserving level set method are compared with those obtained by the algebraic VOF algorithm, which is known as the tangent of hyperbola for interface capturing with the slope weighting (THINC/SW) scheme [13] described in Appendix A, to validate the abilities of the proposed scheme to accurately predict interface of a bubble bursting at a free surface. In addition, our purpose is to understand the effect of surface tension on the behavior of bubble breakup. Three dimensional single bubble rising problem is considered in Section 4.2.3. In Section 4.2.4, we simulate the merge of two bubbles. In Section 4.2.5, three dimensional bubble bursting at a free surface is also investigated.

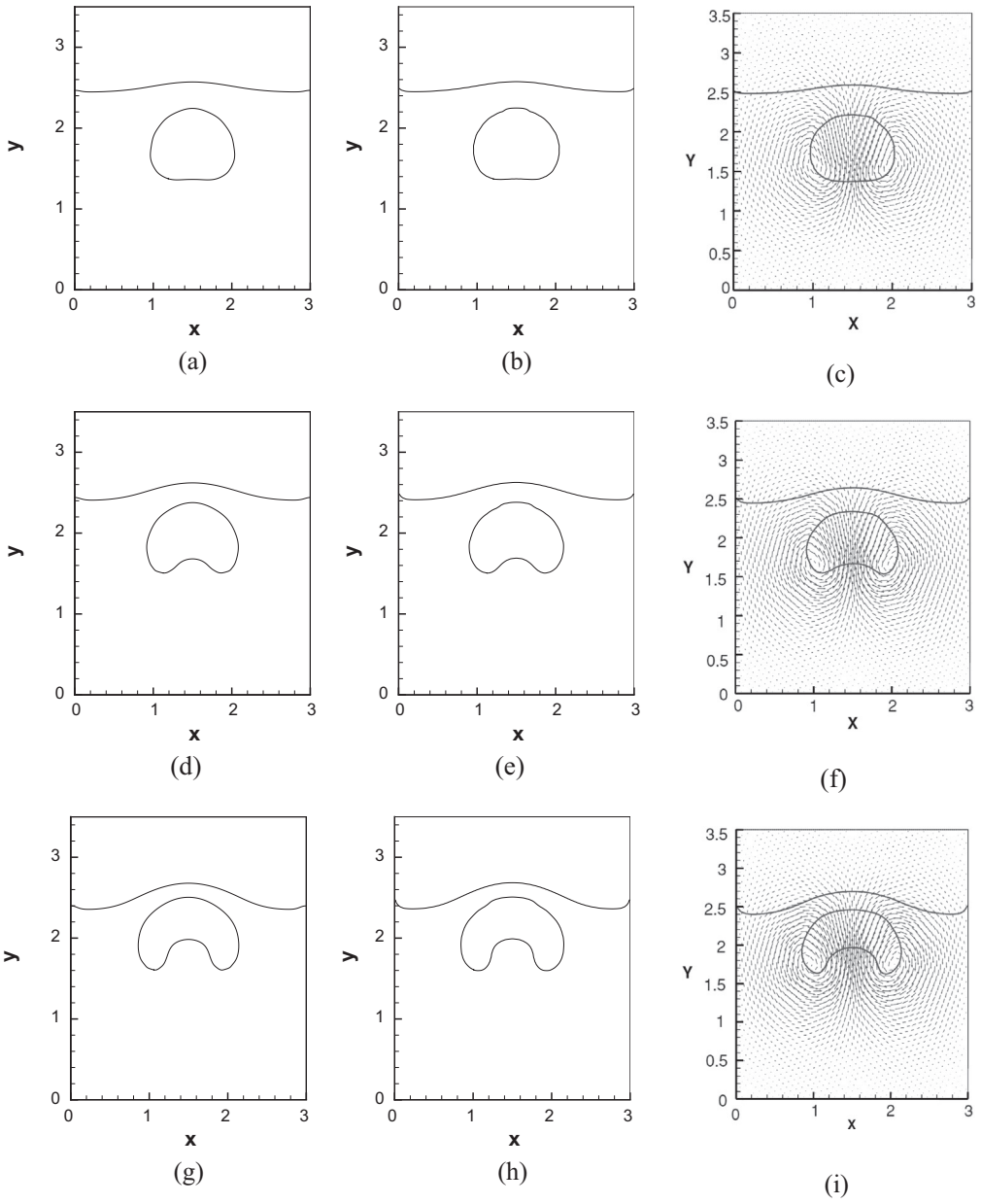

Fig. 11. The predicted results in 180×210 grids for a single bubble rising problem for the case with $Re = 100, \frac{\rho_G}{\rho_L} = 0.5$ and $\frac{\mu_G}{\mu_L} = 0.5$ at different dimensionless times. (a) $t = 1.5$ (LS); (b) $t = 1.5$ (THINC/SW); (c) $t = 1.5$ [48]; (d) $t = 2.0$ (LS); (e) $t = 2.0$ (THINC/SW); (f) $t = 2.0$ [48]; (g) $t = 2.5$ (LS); (h) $t = 2.5$ (THINC/SW); (i) $t = 2.5$ [48]; (j) $t = 3.0$ (LS); (k) $t = 3.0$ (THINC/SW); (l) $t = 3.0$ [48]; (m) $t = 3.5$ (LS); (n) $t = 3.5$ (THINC/SW); (o) $t = 3.5$ [48]; (p) $t = 4.0$ (LS); (q) $t = 4.0$ (THINC/SW); (r) $t = 4.0$ [48].

4.1. Benchmark problems for the proposed level set method

To evaluate the proposed advection algorithm for solving the level set equation, the results obtained from the present scheme for the vortex in a box [1,20,23] and Zalesak's [1,22] problems were compared with those of other existing schemes.

4.1.1. Vortex in a box

This problem can be used to evaluate the accuracy of the predicted interface advection and deformation. The flow field was reversed at $t = T = 1$ so that the exact solution obtained at $t = 2T$ should coincide with its initial solution given by

$$(x - 0.5)^2 + (y - 0.75)^2 = 0.0225. \tag{30}$$

The velocity fields are given as

$$u = \sin^2(\pi x)\sin(2\pi y), \tag{31}$$

$$v = -\sin^2(\pi y)\sin(2\pi x). \tag{32}$$

The numerical results obtained on the uniform grid size of 128×128 at $t = 0.5, t = 1.0$ and $t = 2$ with $\Delta t = 0.01\Delta x$ are compared with the existing level set method introduced by Olsson and Kreiss [23]. In Fig. 1. the proposed level set method is seen to be able to preserve the areas of the filaments much better than the level set method in [23]. For showing the advantages of the proposed improved interface level set method, the stretching process of interface with/without performing intermediate step, which is described in Section 2.2.2, in 128×128 grids is shown in Fig. 2. It is clear that the computed solution using the scheme involving intermediate step can sharply resolve the solution within a thin and elongated filament.

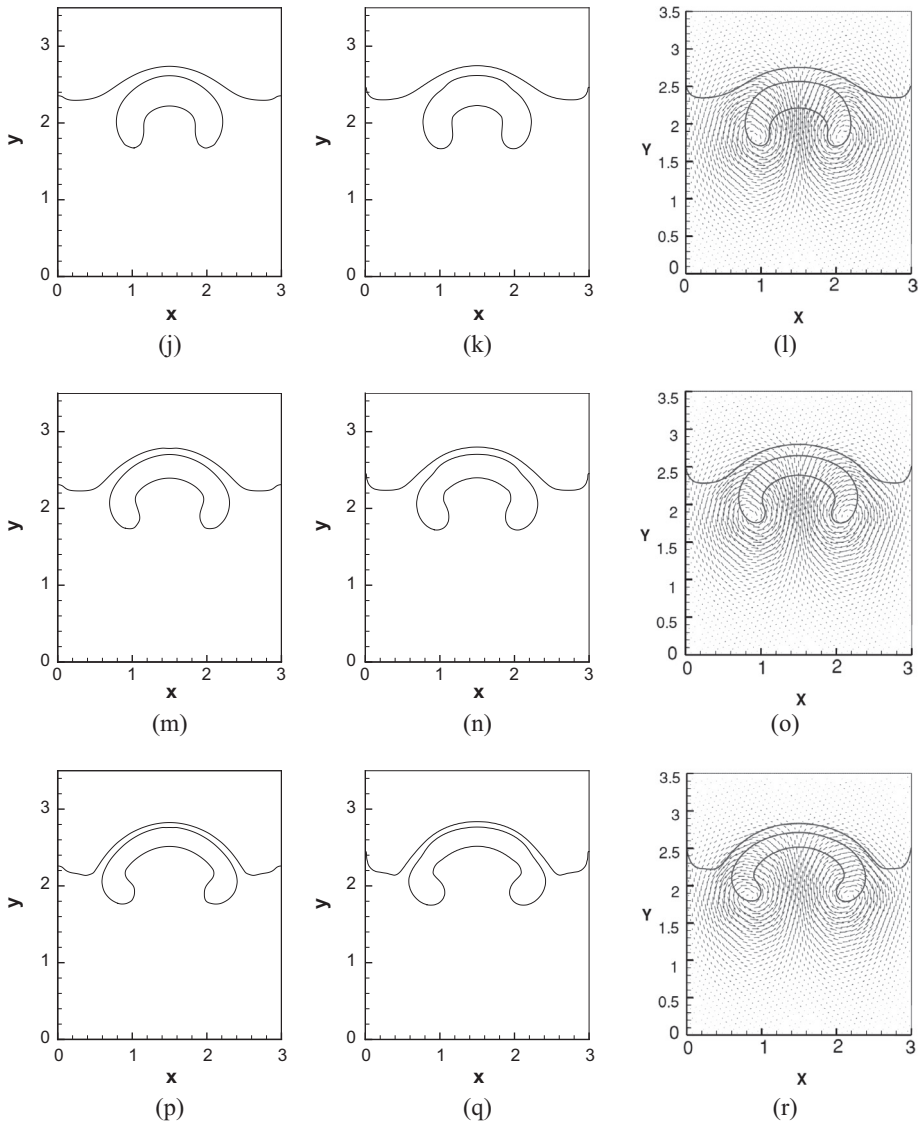

Fig. 11 (*continued*)

4.1.2. Zalesak's problem

In this problem the slotted disk with a radius of 15 and a slot width of 6 is located at (50,75) in the domain $[100 \times 100]$, within which there is a constant angular velocity field

$$u = \frac{\pi(50 - y)}{314}, \tag{33}$$

$$v = \frac{\pi(x - 50)}{314}. \tag{34}$$

Note that the disk returns to its original position for every 200π time units. For the sake of comparison of our results with those of Pijl et al. [22], a uniform grid of 100×100 and $\Delta t = 0.25\Delta x$ is employed to simulate this problem with/without mass correction (i.e. with/without performing intermediate step). Fig. 3 shows that the sharp corner is matched well with that of the initial one when the intermediate step is used. We then simulate this problem in 200×200 grids to measure the effect with/without performing intermediate step after one revolution. In Fig. 4, good agreement with the exact solution is clearly demonstrated.

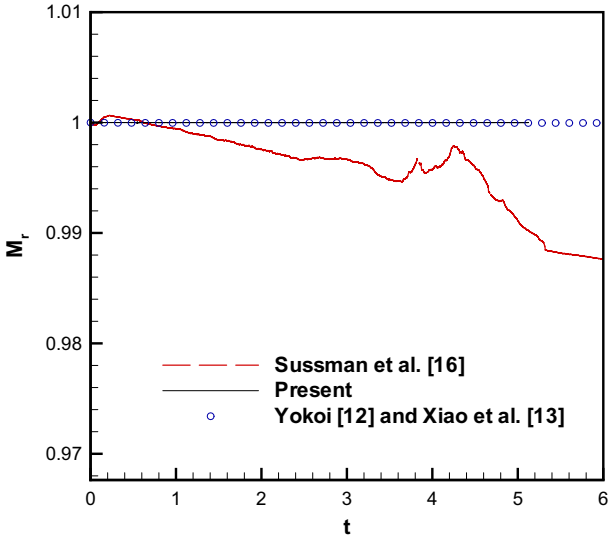

Fig. 12. The mass conservation ratios $\mathbf{M}_r$ definedin Eq. (38) are plotted with respect to the dimensionless time t.

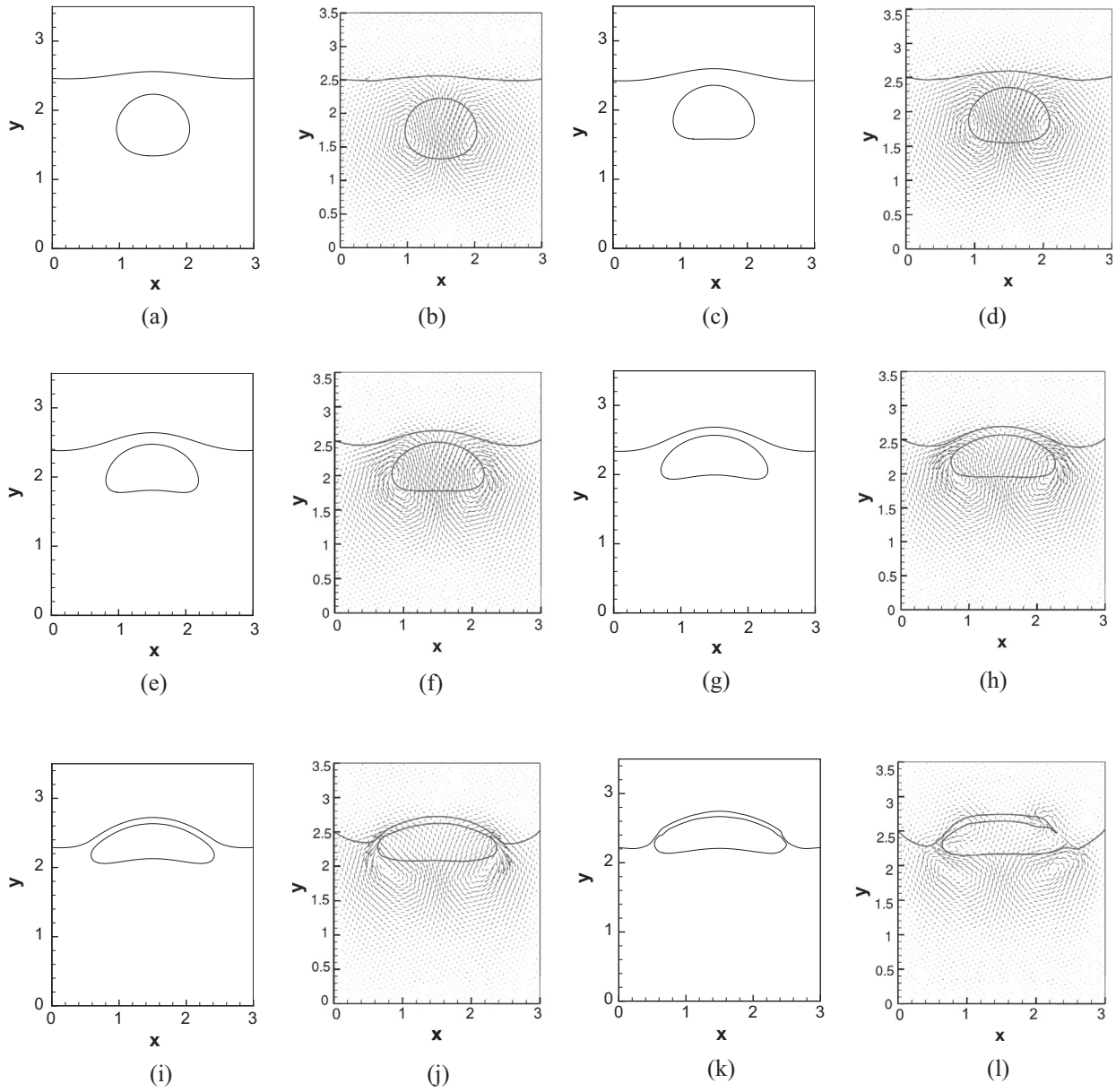

Fig. 13. The predicted results in 210×240 grids for a bubble rising in a container partially filled with water for the case investigated at $Re = 100, We = 10, \frac{\rho_{air}}{\rho_{water}} = 0.5$ and $\frac{\mu_{air}}{\mu_{water}} = 0.5$ at different dimensionless times. (a) $t = 1.5$; (b) $t = 1.5$ [48]; (c) $t = 2.0$; (d) $t = 2.0$ [48]; (e) $t = 2.5$; (f) $t = 2.5$ [48]; (g) $t = 3.0$; (h) $t = 3.0$ [48]; (i) $t = 3.5$; (j) $t = 3.5$ [48]; (k) $t = 4.0$; (l) $t = 4.0$ [48].

4.2. Evaluation of two-phase flow model

To quantitatively evaluate the performance of the proposed level set scheme in resolving the rising interface in viscous fluid, the benchmark quantities including the center of mass, circularity, and rise velocity are investigated [45–47]. The translation of bubble can be measured by the center of mass which is defined as:

$$\mathbf{X}_c = (x_c, y_c) = \frac{\int_{\Omega_b} \mathbf{x} dx}{\int_{\Omega_b} dx}, \tag{35}$$

where Ω_b is the region of bubble. Note that x_c and y_c are the coordinates of the center of mass in x-direction and in y-direction, respectively. The circularity is defined as:

$$\mathbf{C}_l = \frac{P_a}{P_b}, \tag{36}$$

where P_a denotes the perimeter of the initial round bubble and P_b is the bubble perimeter. The rise velocity is defined as

$$\mathbf{V_r} = \frac{\int_{\Omega_b} v dy}{\int_{\Omega_b} dy}, \tag{37}$$

where v is the y-direction velocity magnitude. The ratio of the initial mass predicted at time t is defined below

$$\mathbf{M}_r = \frac{\int_{\Omega} \mathcal{H}(\phi, t) d\Omega}{\int_{\Omega} \mathcal{H}(\phi, t = 0) d\Omega}. \tag{38}$$

4.2.1. Two dimensional single bubble rising problems

A circular bubble of radius 0.0025 m and center (0.005 m, 0.005 m) located in a computational domain $[0, 0.01\,\text{m}] \times [0, 0.02\,\text{m}]$ is considered. Taking $u_r = 0.1\ \frac{\text{m}}{\text{s}}, l_r = 0.005$ m, $\rho_r = 1000\ \frac{\text{kg}}{\text{m}^3}, \mu_r = 0.001\ \frac{\text{N s}}{\text{m}^2}, \rho_r = 0.001 \frac{\text{N s}}{\text{m}^2}$ and $\sigma = 0.0073\ \frac{\text{N}}{\text{m}}$ as the referenced values for the respective velocity, length, density, viscosity and surface tension coefficient, three dimensionless parameters, namely, the Reynolds number (Re), Weber number

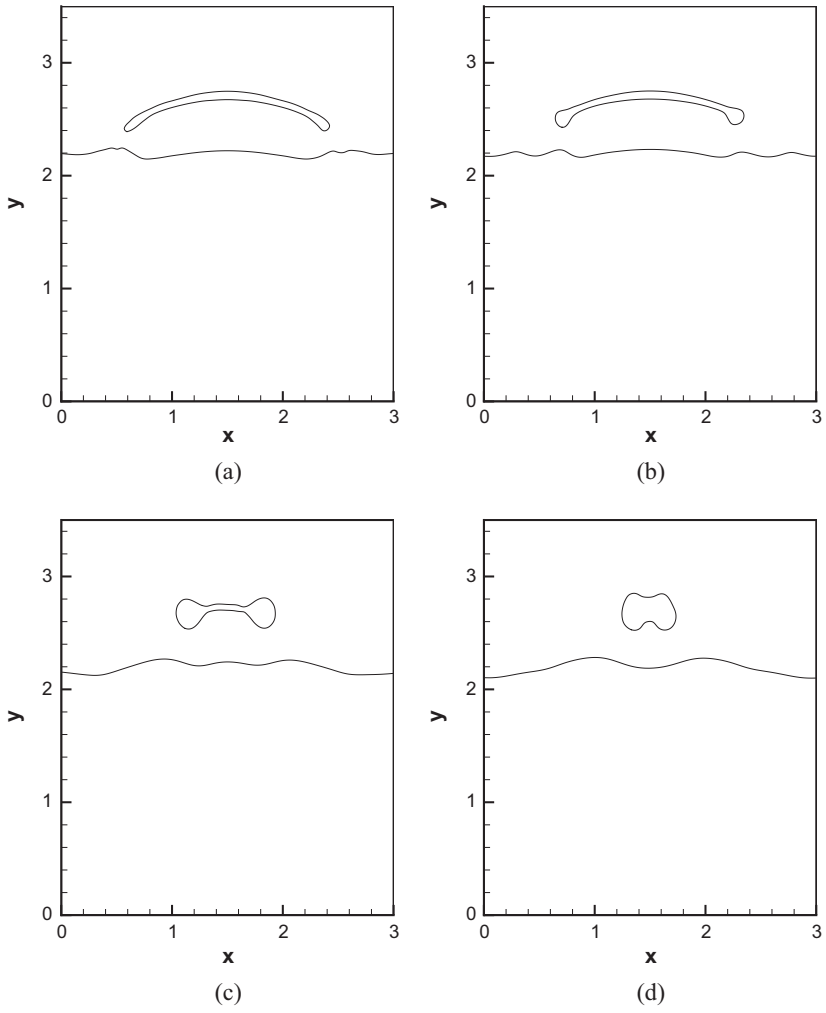

Fig. 14. The time-evolving interfaces for a bubble rising in a container partially filled with water predicted at different times. (a) $t = 4.125$; (b) $t = 4.25$; (c) $t = 4.75$; (d) $t = 5.0$.

(We) and the Froude number (Fr) are $500, 0.68$ and 0.45, respectively. The water–air density and viscosity ratios are specified respectively as $\frac{\rho_L}{\rho_G} = 0.0013$ and $\frac{\rho_L}{\rho_G} = 0.016$. The results will be predicted in the domain containing $50 \times 100, 100 \times 200, 200 \times 400$ grids. Fig. 5 shows that the present result of bubble shape and the numerical result obtained by Olsson and Kreiss [23] are matched very well. The rise velocity, center of mass, circularity and mass ratio are shown in Fig. 6. The reference solution is chosen to be the one computed from the finest grid 200×400. The computed rise velocity in Fig. 6(a) matches well with Olsson and Kreiss in[23]. Also, in Fig. 6(d), the mass is conserved using the proposed level set method. We also provide CPU times obtained with/without performing intermediate step for the proposed level set method in Table 1. The price paid to conserve mass through the use of intermediate solution step is not considerable.

The effect of density for a single rising bubble problem, which has been considered by Zhao et al. [48], is also studied. The tank with $4D$ in length and $6.48D$ in height, where D is the diameter of the initial circular bubble. The air bubble with the radius of $1.0D$ is located at a location that is $1.48D$ above the bottom of the container. The Reynolds number Re, Weber number We, and the density ratio under investigation are $100, 200$ and 0.01, respectively. The predicted time-evolving bubble interfaces in 150×243

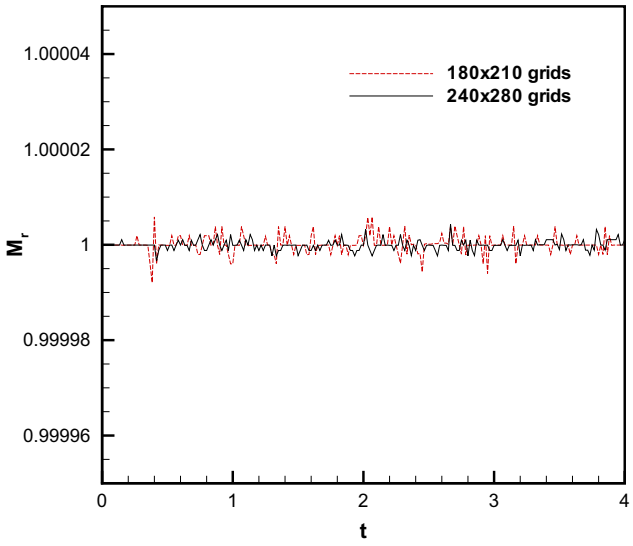

Fig. 15. The ratios of $\mathbf{M}_r$ defined in Eq. (38) are plotted with respect to the dimensionless time t for the calculations carried out in two grids.

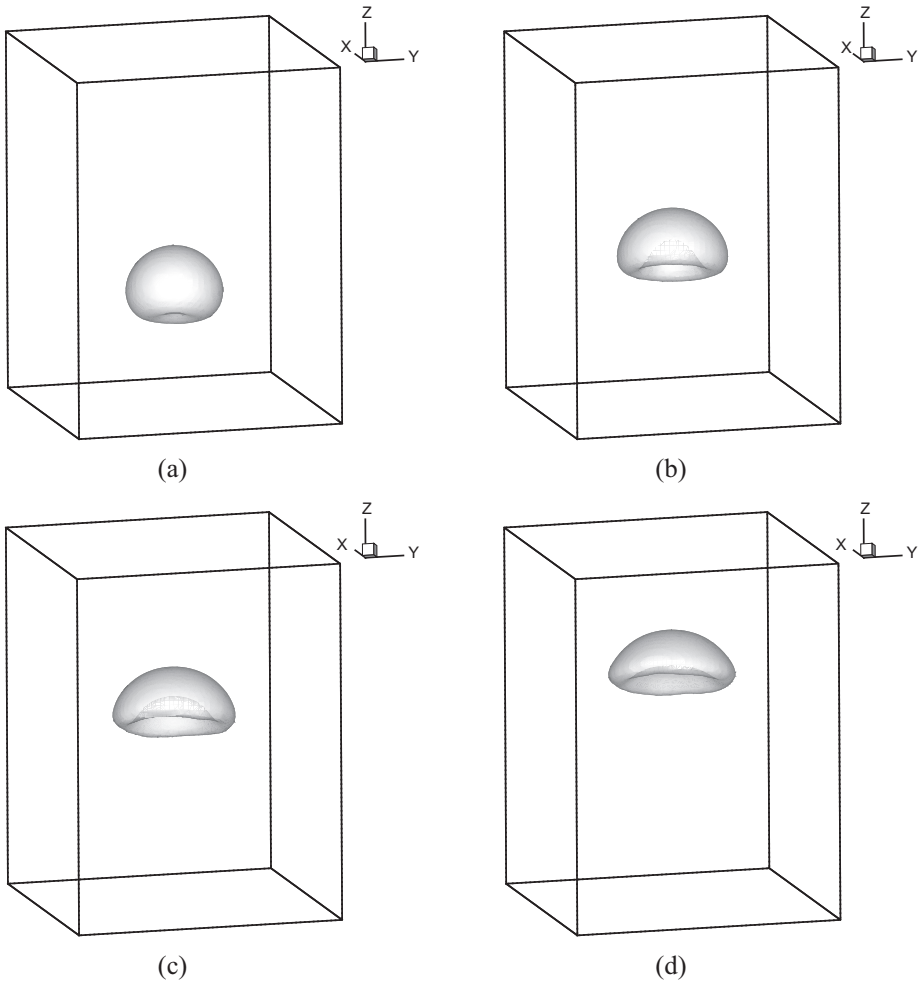

Fig. 16. The predicted results at different dimensionless times for the bubble bursting at a free surface. (a) $t = 0.8$; (b) $t = 1.8$; (c) $t = 2.4$; (d) $t = 3.6$.

grids are plotted in Fig. 7. It is clearly shown that the presently predicted interface topologies agree well with those predicted by Zhao et al. [48]. The predicted mass shown in Fig. 8 is preserved quite well using the present level set method.

The next investigation considers three dimensionless parameters for characterizing the flow motion are chosen as $Re = 100, We = 200$ and density ratio 0.2. The predicted time-evolving bubble interfaces in Fig. 9, plotted at the dimensionless times $t = 1, t = 2, t = 3, t = 4, t = 5.5$ and $t = 6$, are also compared well with those given in Zhao et al. [48]. The numerical results plotted in Fig. 7 and Fig. 9 show that the bubble rises faster because of the decreasing density ratio. In Fig. 10, the degree of mass conservation in comparison with that of the conventional level set method remains very high.

4.2.2. Two dimensional bubble bursting at a free surface

Bubble rising from rest in the incompressible flow subject to buoyancy force has been intensively studied and has many available numerical results in the literature [48,49]. The stationary bubble is centered at $(1.5D, 1.5D)$ in a container of width $3D$ and height of $3.5D$, where D is the initial diameter of the bubble. The initial water depth in the container is $2.5D$. Slip conditions are specified along the horizontal and vertical walls. The air–water density and viscosity ratios are specified as $\rho_G/\rho_L = 0.5$ and $\mu_G/\mu_L = 0.5$, respectively. The case without consideration of surface tension is first investigated at the Reynolds number of $Re(= \frac{\rho UD}{\mu}) = 100$, where $U(= \sqrt{gD})$ is the characteristic velocity. Fig. 11 shows the predicted and numerical results of Zhao et al. [48] at different times. The shape of the bubble is deformed to a kidney shape without taking the surface tension force into account. Also, we show that the presently predicted interface topologies in Fig. 11 agree fairly well with that predicted by the THINC/SW scheme [13]. For simplicity, t, x, y normalized by $\frac{U}{D}, D, D$, respectively, are the dimensionless variables. Conservation of mass has been demonstrated in Fig. 12.

Since surface tension plays an ineligible role in the process of bubble rising, we attempt to simulate this time-evolving bubble problem by taking into account the surface tension force, which corresponds to the Weber number $We\left(= \frac{\rho U^2 D}{\sigma}\right) = 10$, at $Re = 100$. In Fig. 13, the numerical results of the bubble rising problem are plotted against time for the cases with consideration of surface tension effect. Good agreement with the numerical result of Zhao et al. [48] can be seen in Fig. 13. As Fig. 11 and Fig. 13 show, the effect of surface tension force can be observed when t is greater than 1.5. It is worthy to note that in Fig. 13(k) the interface predicted at $t = 4$ is symmetrical using the present mathematical model while interface is asymmetrically, shown in Fig. 13(l), by using the mathematical model of Zhao et al.. The detailed phenomena of bubble breakup are plotted in Fig. 14 in $4.1 \leqslant t \leqslant 5.0$. Uniform grid sizes of 180×210 and 240×280 are used to investigate the effect of grid dependence on the conservative property. The conservative property built in the present level set

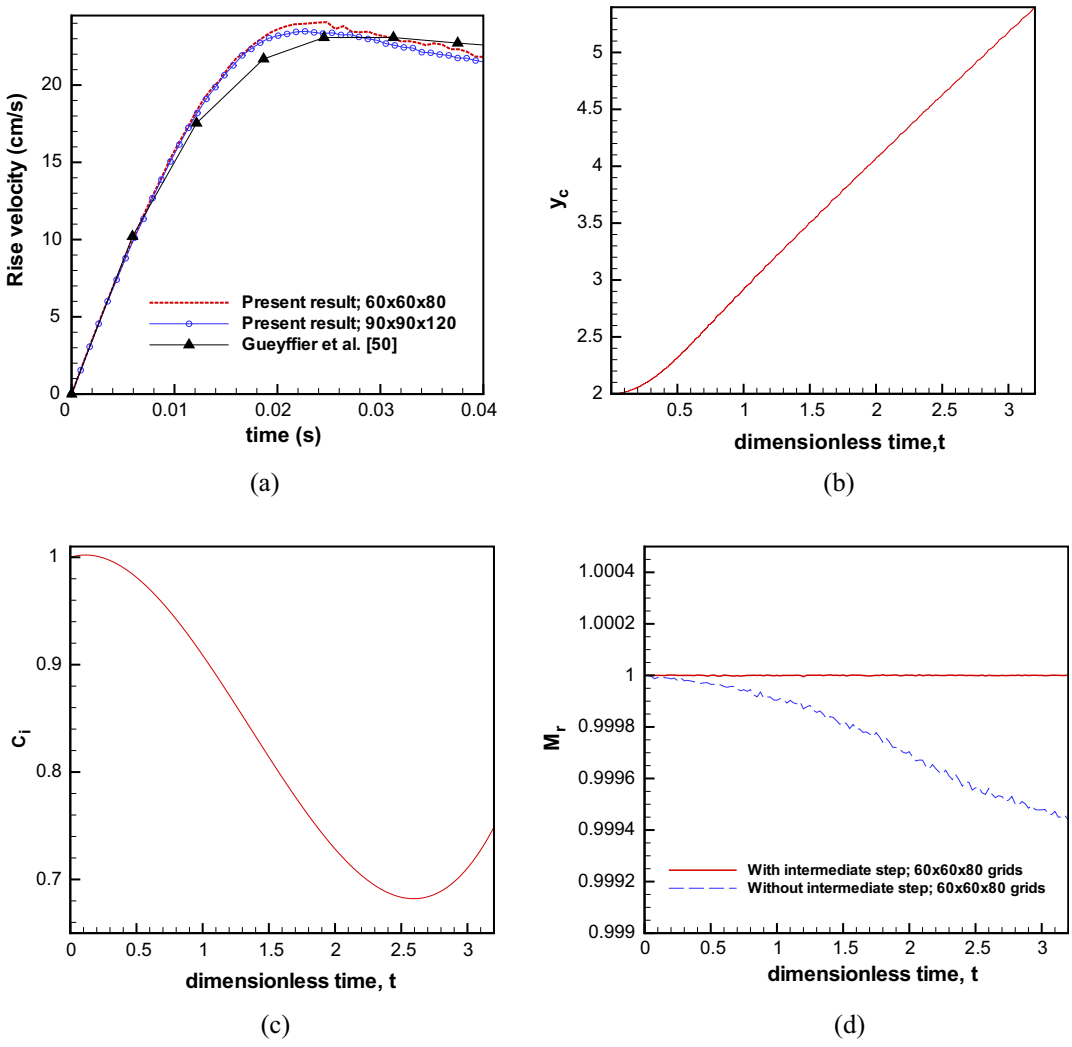

Fig. 17. The plot of the predicted benchmark quantities for the 3D bubble rising problem described in Section 4.2.3. (a) rise velocity; (b) center of mass; (c) circularity; (d) mass ratio.

method is still well retained based on the results computed in different grids in Fig. 15.

4.2.3. Three dimensional single bubble rising problem

The numerical results of the three dimensional single bubble rising problem [50] are available for making a direct comparison. In the current calculation, the bubble has a radius R equal to 1.0 and is placed inside a $6 \times 6 \times 8$ box. The results are predicted at $Re = 9.8, We = 7.6$ and $Fr = 0.76$ in the domain containing $60 \times 60 \times 80$ grids. The predicted bubble rising process is plotted against the dimensionless times $t = 0.8, t = 1.6, t = 2.4$ and $t = 3.6$ in Fig. 16. Benchmark quantities against dimensionless time are shown in Fig. 17. Good agreement with the numerical result of rise velocity in Fig. 17(a) is clearly demonstrated. CPU times are provided with/without performing intermediate step for the proposed level set method in Table 2.

4.2.4. Three dimensional two-bubble merger problem

The merger of two spherical bubbles of the radius $R(= 1)$ is simulated coaxially and obliquely in the domain of $[0, 4R] \times [0, 4R] \times [0, 8R]$ with the Reynolds number of $Re = 67.27$, Weber number of $We = 16$, and the Froude number of $Fr = 1$ [51]. For the coaxial bubble case, the center of the upper bubble is at $(2R, 2R, 2.5R)$ and the center of the lower bubble is at $(2R, 2R, 1R)$. Simulation is carried out in $80 \times 80 \times 160$ grids. The density and viscosity ratios are chosen to be $\rho_G/\rho_L = 0.001$ and $\mu_G/\mu_L = 0.01$, respectively. Good agreement with the experimental observation by Brereton and Korotney [52] and the numerical results by Annaland et al. [10] can be seen in Fig. 18. The deformation and acceleration of the lower bubble in z-direction can be seen when the lower bubble enters into the wake region of upper bubble. The reason for this observation is that the drag force on lower bubble becomes smaller than the upper bubble before the coalescence the two bubbles [4].

For the oblique bubble problem, the center of upper bubble is $(2R, 2R, 2.5R)$ and the center of lower bubble is $(2.85R, 2R, 1R)$. The numerical results predicted in the $256 \times 80 \times 80$ mesh are plotted in Fig. 19. From Fig. 19, we know that the present level set method has been justified owing to the good agreement between our solutions and the solutions obtained in [52,10]. In Fig. 20, the conservative property built in the present level set method is still well retained for both of the coaxial and oblique bubble rising cases.

4.2.5. Three dimensional bubble bursting at a free surface

Numerical simulation of bubble bursting at a free surface has been investigated by Boulton-Stone and Blake [53]. However, they only simulated the air bubble bursting phenomena just before the pinch-off liquid jet. A spherical bubble with unit radius is initially located at $(x, y, z) = (0, 0, -3.2)$ in the domain of

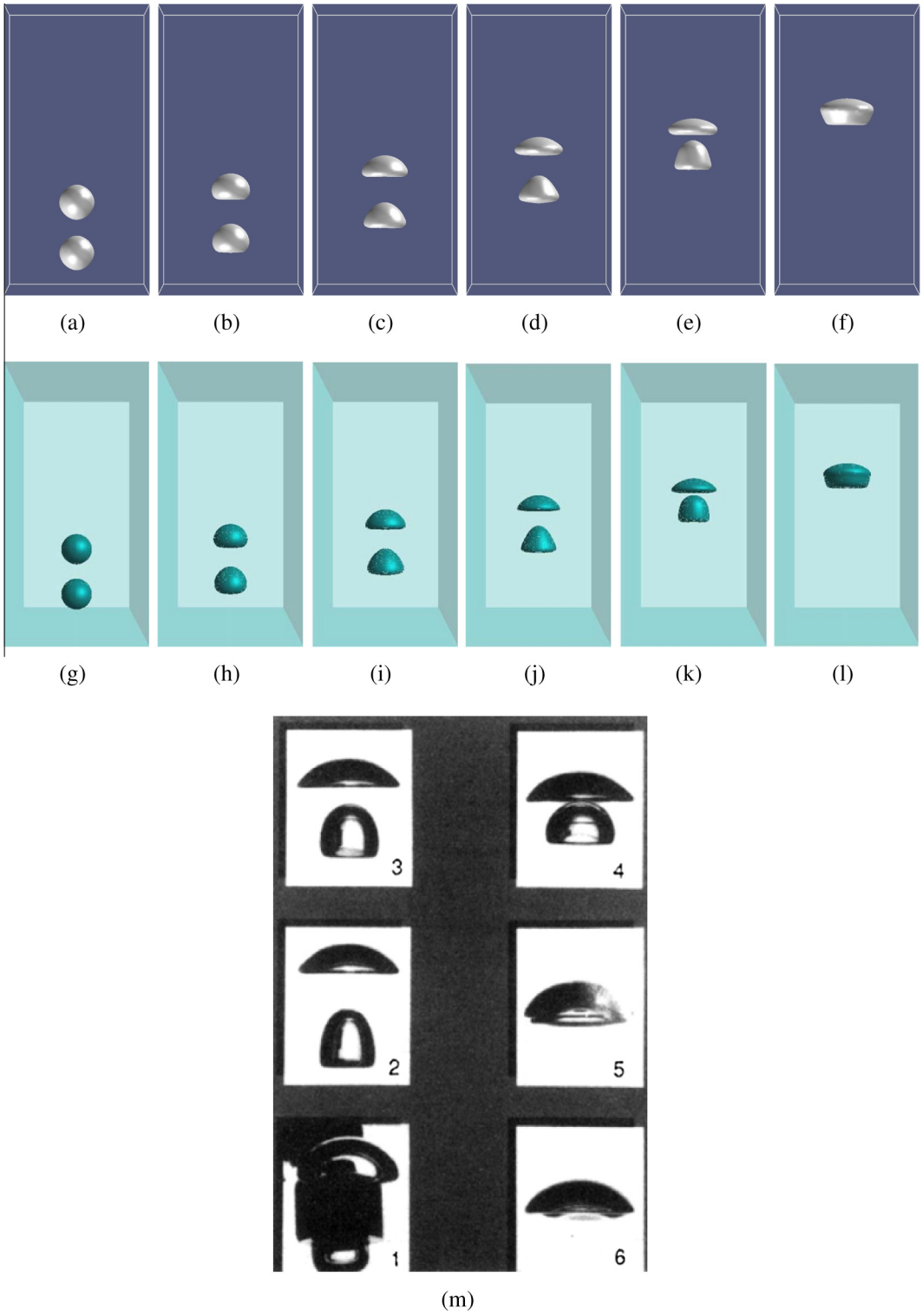

Fig. 18. Comparison of the presently predicted bubble shapes with other numerical and experimental results (time difference between the subsequent photographs is 0.03 s). (a) $t = 0.000$ s (LS); (b) $t = 0.025$ s (LS); (c) $t = 0.050$ s (LS); (d) $t = 0.075$ s (LS); (e) $t = 0.100$ s (LS); (f) $t = 0.125$ s (LS); (g) $t = 0.000$ s [51]; (h) $t = 0.025$ s [51]; (i) $t = 0.050$ s [51]; (j) $t = 0.075$ [51]; (k) $t = 0.100$ s [51]; (l) $t = 0.125$ s [51]; (m) experimental results of [52].

$[-2, 2] \times [-2, 2] \times [-6, 6]$. No-slip boundary conditions are specified on the walls of the box. The dimensionless parameters are set at $Re = 50, We = 1.25$ and $Fr\left(= \frac{U}{\sqrt{gR}}\right) = 1$, where R is the radius of spherical bubbles and is considered as the characteristic length. The air–water density ratio and the viscosity ratio are taken to be 0.001 and 0.01, respectively. The numerical results obtained at different times in $110 \times 110 \times 220$ grids are presented in Fig. 21. We observe that liquid jet starts breaking up into a droplet at $t = 1.5$ in Fig. 21(h) and then the second droplet is formed at $t = 1.8$ in Fig. 21(i). In other words, the liquid jet pinch-off process and the generation of liquid droplets after liquid jet break up due to capillary instability [30] have been accurately predicted using the present level set method.

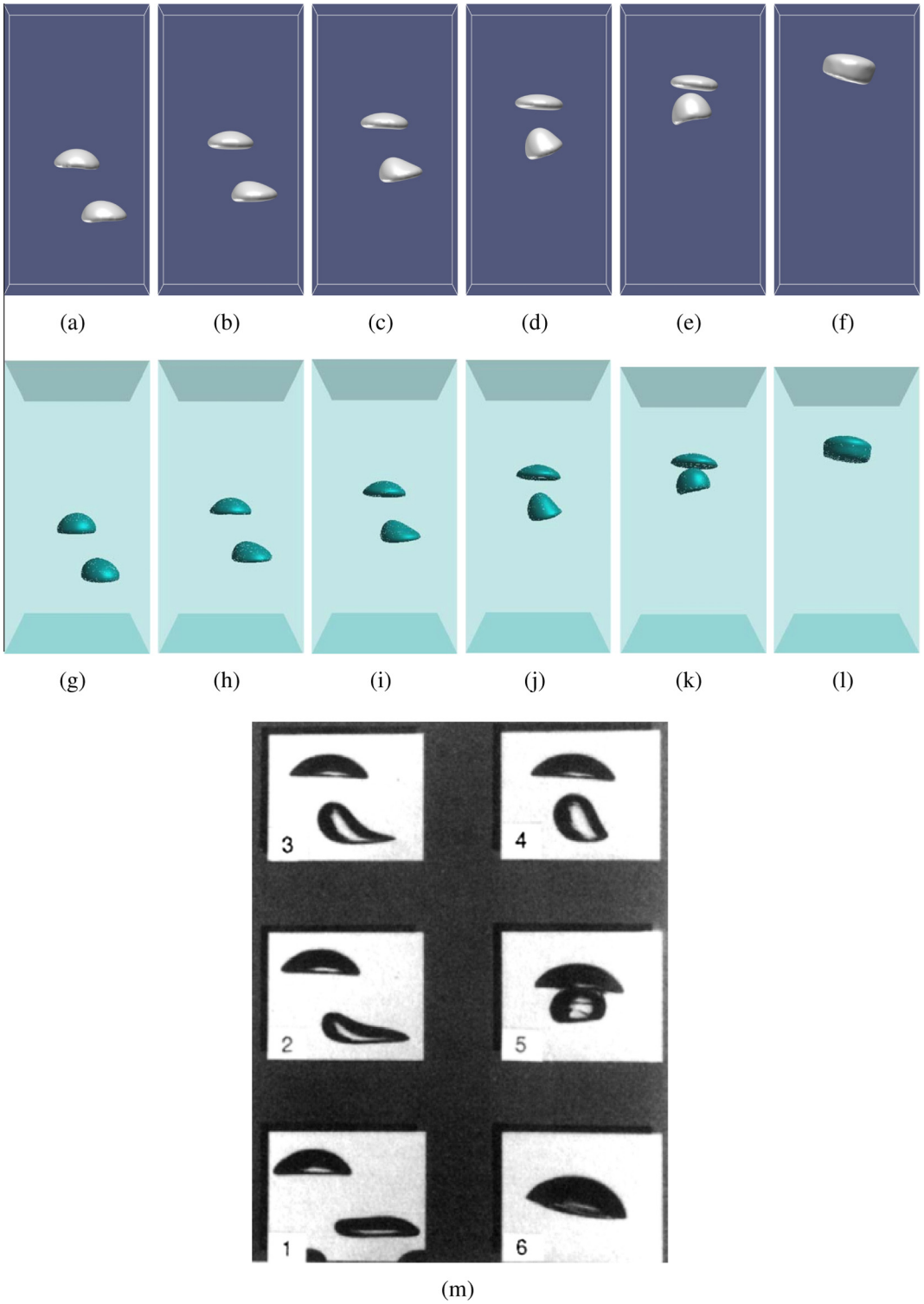

Fig. 19. Comparison of the presently predicted bubble shapes with other numerical and experimental results (time difference between the subsequent photographs is 0.03 s). (a) $t = 0.060$ s (LS); (b) $t = 0.085$ s (LS); (c) $t = 0.110$ s (LS); (d) $t = 0.135$ s (LS); (e) $t = 0.160$ s (LS); (f) $t = 0.185$ s (LS); (g) $t = 0.050$ s [51]; (h) $t = .075$ s [51]; (i) $t = 0.100$ s [51]; (j) $t = 0.125$ s [51]; (k) $t = 0.150$ s [51]; (l) $t = 0.175$ s [51]; (m) experimental results of [52].

5. Concluding remarks

This paper presents an improved interface preserving level set method for investigating the 2D and 3D bubble flow dynamics on fixed Cartesian grids. The interface is moved implicitly by the advection of level set function ϕ, which is split into three solution steps. First, ϕ is computed using the TVD Runge–Katta temporal scheme and the spatial WENO scheme is applied to capture interface excellently. Secondly, the level set function ϕ_{new} is evaluated from the new smoothed Heaviside function. Finally, the correction

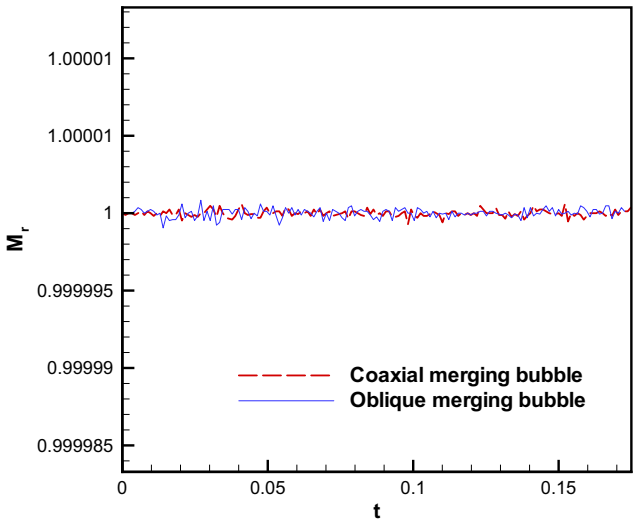

Fig. 20. The ratios $\mathbf{M}_r$ defined in Eq. (38) are plotted with respect to the dimensionless time t for the problem of two merging bubbles.

term is added to the re-initialization equation to keep ϕ_{new} as a distance function and to conserve mass in the sharp interface region. Numerical results show that this improved method can be used to tackle problems with large density ratio, calculate the curvature of bubble surface accurately and can, more importantly, guarantee mass conservation. For the prediction of bubble bursting at a free surface, this method can capture a large topological change such as the splitting and merging of bubbles. In addition, we apply the proposed method with the algebraic VOF algorithm (THINC/SW scheme) to simulate bubble motion without considering surface tension force. Numerical results show that both approaches can conserve mass well, in addition to the prevention of spurious oscillations generated from the moving interface. For the single bubble rising problem, two density ratios $\rho_{\text{ratio}} = 0.2$ and 0.01 are investigated. Bubble rises faster at the high density ratio $\rho_{\text{ratio}} = 0.01$ since the effect of buoyancy influences the motion of a single bubble. Good mass conservation feature is also demonstrated. The interaction of two equal sized rising spherical bubbles under the influence of buoyancy force is investigated. Simulations revealed the coalescence behaviors which are similar to the experimental observation. Numerical results of the final case show that the proposed improved level set method can be easily extended to simulate the three-dimensional problem. Also, bubble deformation can be accurately predicted using the proposed level set method.

6. Acknowledgement

This study was partially supported by the National Natural Science Foundation of China (51479175), Zhejiang Provincial Natural Science Foundation of China (Grant No. LR16E090002) and Fundamental Research Funds for the Central Universities (2014QNA4030).

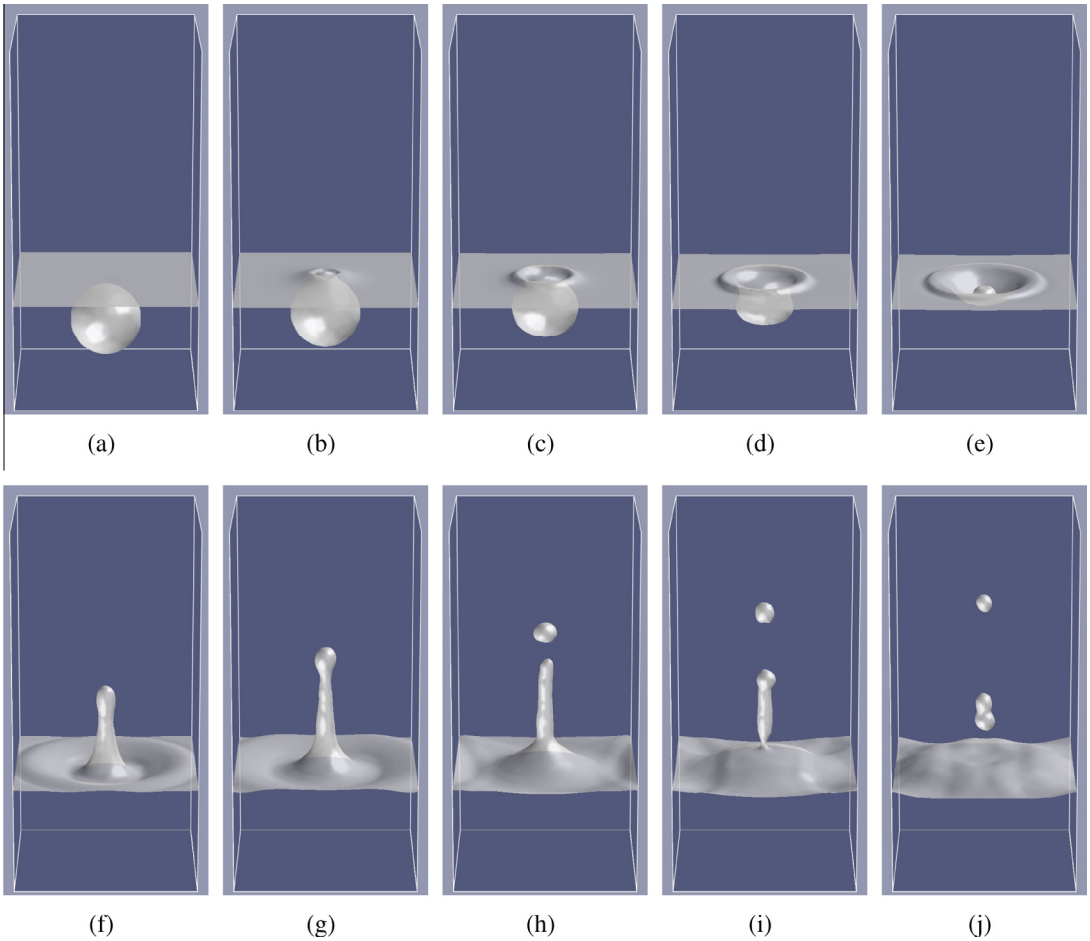

Fig. 21. The predicted results at different dimensionless times for the bubble bursting at a free surface. (a) $t = 0$; (b) $t = 0.2727$; (c) $t = 0.3818$; (d) $t = 0.49$; (e) $t = 0.6$; (f) $t = 0.9272$; (g) $t = 1.2$; (h) $t = 1.5$; (i) $t = 1.8$; (j) $t = 2.1$.

Appendix A. Introduction to VOF type THINC/SW scheme

The THINC/SW [13] scheme is an algebraic VOF type algorithm developed from the THINC scheme [11]. A variable steepness parameter is adopted instead of the constant steepness parameter used in the original THINC scheme. Inclusion of this variable parameter helps maintaining the thickness of the jump transition layer. The THINC/SW scheme is extremely simple but highly accurate in comparison with other conventional VOF schemes. The 1-D advection of the VOF function F is written in a conservation form as follows:

$$\frac{\partial F}{\partial t}+\nabla(uF)=F\frac{\partial u}{\partial x}. \tag{39}$$

Given the cell averaged value $\bar{F}_i^n$ in a cell $x_{i-1/2}, x_{i+1/2}$ at the time step $t=t^n$, the solution of $\bar{F}$ at the $(n+1)$th time step can be computed by

$$\bar{F}_i^{n+1}=\bar{F}_i^n+\frac{1}{\Delta x_i}\left(g_{i+1/2}-g_{i-1/2}\right)+\frac{\Delta t}{\Delta x_i}\bar{F}_i^n\left(u_{i+1/2}^n-u_{i-1/2}^n\right). \tag{40}$$

In the above, $\Delta x_i=x_{i+1/2}-x_{i-1/2}, g_{i+1/2}=\int_{t^n}^{t^{n+1}}(uF)_{i+1/2}dt$ is the flux across the cell boundary $x=x_{i+1/2}$. A reconstruction interpolation function is used in calculating the flux which is expressed as a piecewise hyperbolic tangent function

$$\chi_i=\frac{\alpha}{2}\left\{1+\gamma\tanh\left[\beta\left(\frac{x-x_{i-1/2}}{\Delta x_i}-\delta\right)\right]\right\} \tag{41}$$

The parameters α and γ shown above are specified as

$$\alpha=\begin{cases}\bar{F}_{i+1} & \text{if } \bar{F}_{i+1}\geqslant\bar{F}_{i-1}\\ \bar{F}_{i-1} & \text{otherwise}\end{cases}, \tag{42}$$

$$\gamma=\begin{cases}1 & \text{if } \bar{F}_{i+1}\geqslant\bar{F}_{i-1}\\ -1 & \text{otherwise}\end{cases}. \tag{43}$$

The parameter δ is used to determine the jump center of the hyperbolic tangent function, which is calculated by solving the following equation:

$$\frac{1}{\Delta x_i}\int_{x_{i-1/2}}^{x_{i+1/2}}\chi_i(x)dx=\bar{F}_i^n. \tag{44}$$

The parameter β is introduced to control the slope and thickness of the jump. In the original THINC scheme, a constant value of $\beta=3.5$ is usually used. In THINC/SW scheme, the value of β is adaptively adopted according to the orientation of the interface, thereby improving the ruffling problem involved in the original THINC scheme. For the two dimensional case, β is chosen as

$$\begin{cases}\beta_x=2.3|n_x|+0.01\\ \beta_y=2.3|n_y|+0.01.\end{cases} \tag{45}$$

The normal vector $n=(n_x,n_y)$ is determined by differencing the VOF function $\bar{F}$. After calculating χ_i, the flux $g_{i\pm1/2}$ at the cell boundary can be obtained. Then, the cell integrated value $\bar{F}_i^{n+1}$ is calculated by Eq. (40).

References

[1] B.M. Ningegowda, B. Premachandran, A coupled level set and volume of fluid method with multi-directional advection algorithms for two-phase flows with and without phase change, Int. J. Heat Mass Transfer 79 (2014) 532–550.

[2] S.O. Unverdi, G. Tryggvason, A front-tracking method for viscous, incompressible multi-fluid flows, J. Comput. Phys. 100 (1) (1992) 25–37.

[3] K.M. Shyue, A wave-propagation based volume tracking method for compressible multicomponent flow in two space dimensions, J. Comput. Phys. 215 (1) (2006) 219–244.

[4] I. Chakraborty, G. Biswas, P.S. Ghoshdastidar, A coupled level-set and volume-of-fluid method for the buoyant rise of gas bubbles in liquids, Int. J. Heat Mass Transfer 58 (1) (2013) 240–259.

[5] C.W. Hirt, B.D. Nichols, Volume of fluid (Vof) method for the dynamics of free boundaries, J. Comput. Phys. 39 (1) (1981) 201–225.

[6] W.F. Noh, P.R. Woodward, SLIC (simple line interface method), Proceedings of the Fifth International Conference on Numerical Methods in Fluid Dynamics June 28CJuly 2, 1976 Twente University, Springer Berlin Heidelberg, Enschede, 1976, pp. 330–340.

[7] P. Rauschenberger, B. Weigand, A Volume-of-Fluid method with interface reconstruction for ice growth in supercooled water, J. Comput. Phys. 282 (2015) 98–112.

[8] B. Liu, J. Cai, X. Huai, Heat transfer with the growth and collapse of cavitation bubble between two parallel heated walls, Int. J. Heat Mass Transfer 78 (2014) 830–838.

[9] C.S. Wu, D.L. Young, H.C. Wu, Simulations of multidimensional interfacial flows by an improved volume-of-fluid method, Int. J. Heat Mass Transfer 60 (2013) 739–755.

[10] D.K. Agarwal, S.W.J. Welch, G. Biswas, F. Durst, Planar simulation of bubble growth in film boiling in near-critical water using a variant of the VOF method, J. Heat Transfer 126 (3) (2004) 329–338.

[11] F. Xiao, Y. Honma, T. Kono, A simple algebraic interface capturing scheme using hyperbolic tangent function, Int. J. Numer. Methods Fluids 48 (9) (2005) 1023–1040.

[12] K. Yokoi, Efficient implementation of THINC scheme: a simple and practical smoothed VOF algorithm, J. Comput. Phys. 226 (2) (2007) 1985–2002.

[13] F. Xiao, S. Ii, C. Chen, Revisit to the THINC scheme: a simple algebraic VOF algorithm, J. Comput. Phys. 230 (19) (2011) 7086–7092.

[14] K.M. Shyue, F. Xiao, An Eulerian interface sharpening algorithm for compressible two-phase flow: the algebraic THINC approach, J. Comput. Phys. 268 (2014) 326–354.

[15] S. Ii, K. Sugiyama, S. Takeuchi, S. Takagi, Y. Matsumoto, F. Xiao, An interface capturing method with a continuous function: the THINC method with multi-dimensional reconstruction, J. Comput. Phys. 231 (5) (2012) 2328–2358.

[16] M. Sussman, P. Smereka, S. Osher, A level set approach for computing solutions to incompressible two-phase flow, J. Comput. Phys. 114 (1) (1994) 146–159.

[17] P. Rauschenberger, A. Criscione, K. Eisenschmidt, D. Kintea, S. Jakirlić, Ž. Tuković, I.V. Roisman, B. Weigand, C. Tropea, Comparative assessment of Volume-of-Fluid and Level-Set methods by relevance to dendritic ice growth in supercooled water, Comput. Fluids 79 (2013) 44–52.

[18] K. Yokoi, A variational approach to motion of triple junction of gas, liquid and solid, Comput. Phys. Commun. 180 (7) (2009) 1145–1149.

[19] M.J. Ni, S. Komori, N.B. Morley, Direct simulation of falling droplet in a closed channel, Int. J. Heat Mass Transfer 49 (1) (2006) 366–376.

[20] W.S. Yue, C.L. Lin, V.C. Patel, Numerical simulation of unsteady multidimensional free surface motions by level set method, Int. J. Numer. Meth. Fluids 42 (8) (2003) 853–884.

[21] C.L. Lin, H. Lee, T. Lee, L.J. Weber, A level set characteristic Galerkin finite element method for free surface flows, Int. J. Numer. Meth. Fluids 49 (5) (2005) 521–547.

[22] S.P. van der Pijl, A. Segal, C. Vuik, P. Wesseling, A mass-conserving Level-Set method for modelling of multi-phase flows, Int. J. Numer. Methods Fluids 47 (4) (2005) 339–361.

[23] E. Olsson, G. Kreiss, A conservative level set method for two phase flow, J. Comput. Phys. 210 (1) (2005) 225–246.

[24] E. Olsson, G. Kreiss, S. Zahedi, A conservative level set method for two phase flow II, J. Comput. Phys. 225 (1) (2007) 785–807.

[25] L. Strubelj, I. Tiselj, Two-fluid model with interface sharpening, Int. J. Numer. Methods Eng. 85 (5) (2011) 575–590.

[26] K.C. Ng, Y.H. Hwang, T.W.H. Sheu, C.H. Yu, Moving Particle Level-Set (MPLS) method for incompressible multiphase flow computation, Comput. Phys. Commun. 196 (2015) 317–334.

[27] Y.F. Yap, J.C. Chai, T.N. Wong, K.C. Toh, H.Y. Zhang, A global mass correction scheme for the level-set method, Numer. Heat Transfer Part B: Fundam. 50 (5) (2006) 455–472.

[28] Y. Zhang, Q. Zou, D. Greaves, Numerical simulation of free-surface flow using the level-set method with global mass correction, Int. J. Numer. Meth. Fluids 63 (6) (2010) 651–680.

[29] Y. Zhang, Q. Zou, D. Greaves, D. Reeve, A. Hunt-Raby, D. Graham, P. James, X. Lv, A level set immersed boundary method for water entry and exit, Comput. Phys. Commun. 8 (2) (2010) 265–288.

[30] M. Sussman, E.G. Puckett, A coupled level set and volume-of-fluid method for computing 3D and axisymmetric incompressible two-phase flows, J. Comput. Phys. 162 (2) (2000) 301–337.

[31] I. Chakraborty, G. Biswas, P.S. Ghoshdastidar, Bubble generation in quiescent and co-flowing liquids, Int. J. Heat Mass Transfer 54 (21) (2011) 4673–4688.

[32] Z. Wang, J. Yang, B. Koo, F. Stern, A coupled level set and volume-of-fluid method for sharp interface simulation of plunging breaking waves, Int. J. Multiph. Flow 35 (3) (2009) 227–246.

[33] K. Yokoi, A practical numerical framework for free surface flows based on CLSVOF method multi-moment methods and density-scaled CSF model: numerical simulations of droplet splashing, J. Comput. Phys. 232 (1) (2013) 252–271.

[34] G. Son, N. Hur, A coupled level set and volume-of-fluid method for the buoyancy-driven motion of fluid particles, Numer. Heat Transfer: Part B: Fundam. 42 (6) (2002) 523–542.

[35] G. Son, Efficient implementation of a coupled level-set and volume-of-fluid method for three-dimensional incompressible two-phase flows, Numer. Heat Transfer: Part B: Fundam. 43 (6) (2003) 549–565.
[36] D.L. Sun, W.Q. Tao, A coupled volume-of-fluid and level set (VOSET) method for computing incompressible two-phase flows, Int. J. Heat Mass Transfer 53 (4) (2010) 645–655.
[37] T. Wang, H. Li, Y. Feng, D. Shi, A coupled volume-of-fluid and level set (VOSET) method on dynamically adaptive quadtree grids, Int. J. Heat Mass Transfer 67 (2013) 70–73.
[38] K. Ling, Z.H. Li, D.L. Sun, Y.L. He, W.Q. Tao, A three-dimensional volume of fluid & level set (VOSET) method for incompressible two-phase flow, Comput. Fluids 118 (2015) 293–304.
[39] M. Sussman, E. Fatemi, An efficient, interface-preserving level set redistancing algorithm and its application to interfacial incompressible fluid flow, SIAM J. Sci. Comput. 20 (4) (1999) 1165–1191.
[40] K. Yokoi, A density-scaled continuum surface force model within a balanced force formulation, J. Comput. Phys. 278 (2014) 221–228.
[41] B.P. Leonard, A stable and accurate convective modelling procedure based on quadratic upstream interpolation, Comput. Methods Appl. Mech. Eng. 19 (1) (1979) 59–98.
[42] G.S. Jiang, D. Peng, Weighted ENO schemes for Hamilton–Jacobi equations, SIAM J. Sci. Comput. 21 (6) (2000) 2126–2143.
[43] C.W. Shu, S. Osher, Efficient implementation of essentially non-oscillatory shock-capturing schemes, J. Comput. Phys. 77 (2) (1988) 439–471.
[44] A.J. Chorin, Numerical solution of the Navier–Stokes equations, Math. Comput. 22 (104) (1968) 745–762.
[45] J. Klostermann, K. Schaake, R. Schwarze, Numerical simulation of a single rising bubble by VOF with surface compression, Int. J. Numer. Methods Fluids 71 (2013) 960–982.
[46] S. Hysing, S. Turek, D. Kuzmin, N. Parolini, E. Burman, S. Ganesan, L. Tobiska, Quantitative benchmark computations of two-dimensional bubble dynamics, Int. J. Numer. Methods Fluids 60 (2009) 1259–1288.
[47] J. Hua, J. Lou, Numerical simulation of bubble rising in viscous liquid, J. Comput. Phys. 222 (2) (2007) 769–795.
[48] Y. Zhao, H.H. Tan, B. Zhang, A high-resolution characteristics-based implicit dual time-stepping VOF method for free surface flow simulation on unstructured grids, J. Comput. Phys. 183 (1) (2002) 233–273.
[49] D. Pan, C.H. Chang, The capturing of free surfaces in incompressible multi-fluid flows, Int. J. Numer. Methods Fluids 33 (2) (2000) 203–222.
[50] D. Gueyffier, J. Li, A. Nadim, R. Scardovelli, S. Zaleski, Volume-of-fluid interface tracking with smoothed surface stress methods for three-dimensional flows, J. Comput. Phys. 152 (1999) 423–456.
[51] M. van Sint Annaland, N.G. Deen, J.A.M. Kuipers, Numerical simulation of gas bubbles behaviour using a three-dimensional volume of fluid method, Chem. Eng. Sci. 60 (11) (2005) 2999–3011.
[52] G. Brereton, D. Korotney, Coaxial and oblique coalescence of two rising bubbles, Proceedings of AMD, (1991) 119.
[53] J.M. Boulton-Stone, J.R. Blake, Gas bubbles bursting at a free surface, J. Fluid Mech. 254 (1993) 437–466.